ORIGINAL PAPER

Landslide susceptibility assessment using different rainfall event-based landslide inventories: advantages and limitations

Sérgio C. Oliveira[1,2] · José L. Zêzere[1,2] · Ricardo A. C. Garcia[1,2] · Susana Pereira[1,2,3] · Teresa Vaz[1] · Raquel Melo[1,2]

Abstract

The present work aims to evaluate potential sources of uncertainty associated with rainfall-triggered event-based landslide inventories within the framework of landslide susceptibility assessment. Therefore, this study addresses the following questions: (i) How representative is an event-based landslide inventory map of the total landslide activity and distribution in a study area?; (ii) How reliable is an event-based landslide susceptibility map?; (iii) How appropriate is an event-based landslide inventory map for independently validating a landslide susceptibility map? To address these questions, two independent and contrasting rainfall event-based landslide inventories were used, together with a historical landslide inventory, to assess landslide susceptibility for different types of landslides in a study area located north of Lisbon, Portugal. The results revealed the following findings: (i) contrasting rainfall critical conditions for failure can trigger similar landslide types, although they may vary in size and be spatially constrained by different predisposing conditions, particularly lithology and soil type; (ii) landslide susceptibility models using event-based landslide inventories are not reliable in the study area, regardless of the landslide inventory map used for training and validation; and (iii) complementary sources of uncertainty results from using incomplete historical landslide inventories to assess landslide susceptibility and non-totally independent landslide inventories for modeling validation. The present study enhances the understanding of regional landslide susceptibility patterns based on contrasting rainfall-trigger conditions, providing valuable information to minimize exposure; to design regional landslide early warning systems for specific rainfall-trigger landslide events; and to improve the response and preparedness of civil protection services.

Keywords Landslides · Event-based landslide inventories · Short intense and long-lasting rainfall events · Landslide susceptibility assessment

---

Extended author information available on the last page of the article

\underline{\textcircled{} Springer}

1 Introduction

The availability of complete event-based landslide inventories associated to different rainfall preparatory and triggering conditions is uncommon for a single region. The scarcity of landslide inventory maps associated to different rainfall triggering conditions is frequently highlighted in the literature, even when two independent inventory maps are available for the same region, allowing comparison (Mondini et al. 2014).

Determining the temporal occurrence of landslides is assumed as one of the most critical issues which limits "the performance of a quantitative determination of the probability of slope failure or landslide reactivation within a defined time span" (Corominas et al. 2014). Therefore, assessing the temporal occurrence of landslides is recognized as an important step in evaluating and managing landslide hazard and conducting risk analysis (Corominas et al. 2014). Some of the most important landslide triggering mechanisms are earthquakes (e.g., Harp et al. 2011; Vaz and Zêzere 2016; Chen et al. 2020) and rainfall (e.g., Su et al. 2015; Zêzere et al. 2015; Pereira et al. 2017; Vaz et al. 2018; Gariano et al. 2021). The landslide inventory map provides information on the location of landslides and their main characteristics over a territory (Pašek 1975; Guzzetti et al. 2000). Different sources are commonly used for landslide mapping: field surveying (Ardizzone et al. 2007; Zêzere et al. 2017), interpretation of aerial photographs (Guzzetti et al. 2000; Santangelo et al. 2015; Oliveira et al. 2017), Light Detection and Ranging (LIDAR) derivate (Ardizzone et al. 2007; Van Den Eeckhaut et al. 2013), or very-high resolution (VHR) monoscopic and stereoscopic satellite images (Ardizzone et al. 2013; Murillo-García et al. 2015; Stumpf et al. 2017).

Frequently, two strategies are used to represent landslides in a map (Sterlacchini et al. 2011; Oliveira et al. 2015a; Zêzere et al. 2017): (i) a single point per landslide, usually the centroid of the landslide area or the centroid of the landslide depletion zone; (ii) a polygon drawing the boundary of each landslide or each landslide depletion zone. The construction of a landslide inventory is data source dependent and time-consuming. According to the data source, landslide inventory maps have been differentiated between landslide archives, which document the location of past landslides from literature or other historical sources, and geomorphological inventory maps (Guzzetti et al. 2000).

In addition, landslide inventories are subdivided into historical, multi-temporal, seasonal and event-based landslide inventory maps (Guzzetti et al. 2012). The main criteria that define these subclasses of landslide inventories are: (i) the landslides association to a single or to multiple landslide events, (ii) the time through which the cumulative effects of landslide events are registered over a region, and (iii) the landslide age (absolute or relative). Historical landslide inventory maps include landslide records spanning from tens to thousands of years, with the age of landslides often not differentiated or expressed in relative terms (e.g., recent, old or very old) (Guzzetti et al. 2012). Multi-temporal landslide inventory maps are derived from landslides that have been triggered by multiple events occurring over extended periods (e.g., years to decades) (Galli et al. 2008). Seasonal landslide inventory maps cover landslides also triggered by multiple events but during a singular season (Fiorucci et al. 2011). Finally, the event-based landslide inventory map reports the landslides associated to a unique natural trigger (Guzzetti et al. 2012). This type of inventory is prepared just after the event to portray the landslide occurrences linked to critical triggering conditions (Ghosh et al. 2012). However, the use of high-resolution/high-quality aerial photographs and satellite images captured shortly after the landslide event, when the evidence of landslides is fresh and

easily recognizable (Guzzetti et al. 2012), enables to obtain reliable event-based landslide inventories even a decade or more after the event has occurred (Oliveira 2012; Zieher et al. 2016).

Focusing on rainfall-triggered landslides, it is expected that different landslide types occur associated to different rainfall critical conditions (e.g., Zêzere et al. 1999b, 2015; Zêzere and Trigo 2011; Martelloni et al. 2012). Although it has been widely acknowledged that landslides can be triggered both by short intense rainfall events and long-lasting rainfall events (Guzzetti et al. 2007; Zêzere et al. 2015), most landslide susceptibility models, based on rainfall event-based landslide inventories found in literature, are related to intense/short duration rainfall critical conditions (a few hours to a few days of rainfall). These conditions typically include intense rainstorms/summer storms (Dai and Lee 2003; Mondini et al. 2011, 2014; Persichillo et al. 2017), typhons (B Lee et al. 2008; Bhandary et al. 2013; Mondini and Chang 2014; Chang et al. 2014; Lee and Chung 2017;) or heavy rainfall events during the monsoon season (Ghosh et al. 2012).

The landslide inventory maps are used to evaluate the extent of landslide phenomena in a region, such as their distribution, the dominant type, the deformation patterns, the recurrence and statistical characteristics of slope failures (Guzzetti et al. 2012). Moreover, landslide inventory maps allow for the assessment of the spatial probability of landslide initiation and runout, as well as the probability of potential landslide sizes for a given return period (Corominas et al. 2014). However, only a limited number of studies have evaluated the direct effects of using different landslide inventories to model landslide susceptibility for the same area (Bornaetxea et al. 2023). Furthermore, the direct effects of using event-based landslide inventories, according to landslide type, for susceptibility assessment have only been investigated in a few cases (e.g. Lee et al. 2008; Chang et al. 2014; Knevels et al. 2020).

To the best of our knowledge, there has been little discussion on the critical rainfall conditions and characteristics of rainfall event-based landslide inventories used to assess landslide susceptibility in this context. Therefore, the aim of this work is to investigate potential sources of uncertainty in landslide susceptibility assessments resulting from the application of rainfall-triggered event-based landslide inventories. This study is designed to address three possible sources of uncertainty: (i) How representative is an event-based landslide inventory map of the total landslide activity and distribution in a study area?; (ii) How reliable can be an event-based landslide susceptibility map?; (iii) How appropriate can be an event-based landslide inventory map to independently validate a landslide susceptibility map?

2 Regional slope instability—data and processes description

2.1 Geology and geomorphology of the study area

The Grande da Pipa River (GPR) basin is located in the north of Lisbon region, Portugal (Fig. 1A). The basin covers an area of 110 km^2 and the elevation ranges from 5 to 440 m. The lithology mainly consists of sedimentary formations dating from the upper Jurassic (LU4–LU10, Fig. 1B covering 95.7% of the study area), with predominance of limestones, marls, mudstones and sandstones intercalations (Kullberg et al. 2006; Zbyszewski and Assunção 1965). Rocks are deformed by a large anticline whose axis is in the central part of the basin (Ribeiro et al. 1979; Zbyszewski and Assunção 1965).
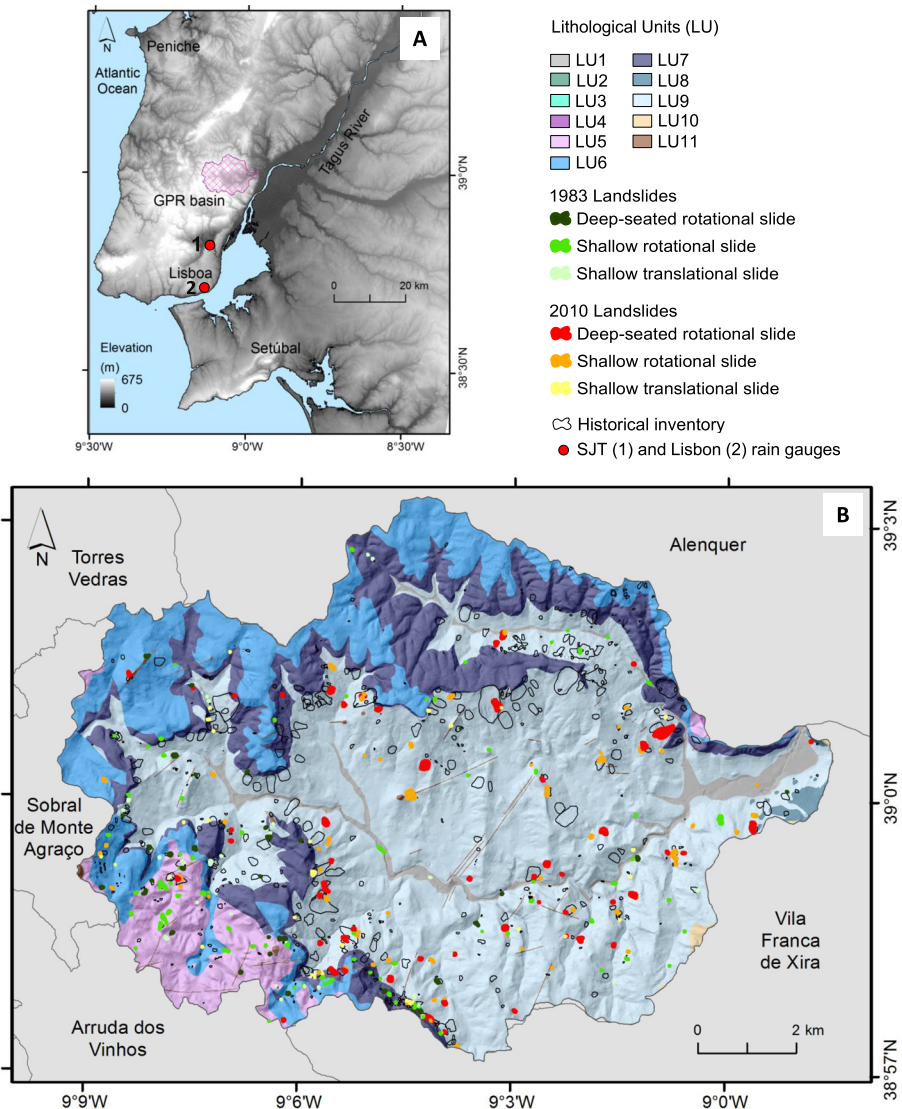
Fig. 1 Grande da Pipa River (GPR) basin location (**A**), Lithological units (LU), 1983 and 2010 rainfall event-based and historical landslide inventories (**B**). Lithological units based uniquely on age criteria: LU1—Alluvium; LU2—Limestone intercalations; LU3—Conglomerates, sandstones, and mudstones; LU4—Sandstones, marls, and limestones; LU5—Limestones and marls; LU6—Mudstones, sandstones, marls, and limestones; LU7—Coralic limestones; LU8—Limestones; LU9—Marls, mudstones, and sandstones; LU10—Conglomerates; LU11—Dykes and magmatic intrusions

Therefore, the bedding planes dip outwards the basin center, creating cuesta-type landforms. The older rocks (LU9—marls, mudstones and sandstone) outcrop in the center of the basin and have been subjected to intense differential erosion during the Quaternary (Ferreira 1984). Above the older rocks there is an open to southeast horse shoe belt of limestone rock walls which are 10–20 m high and produce the steepest slopes in the
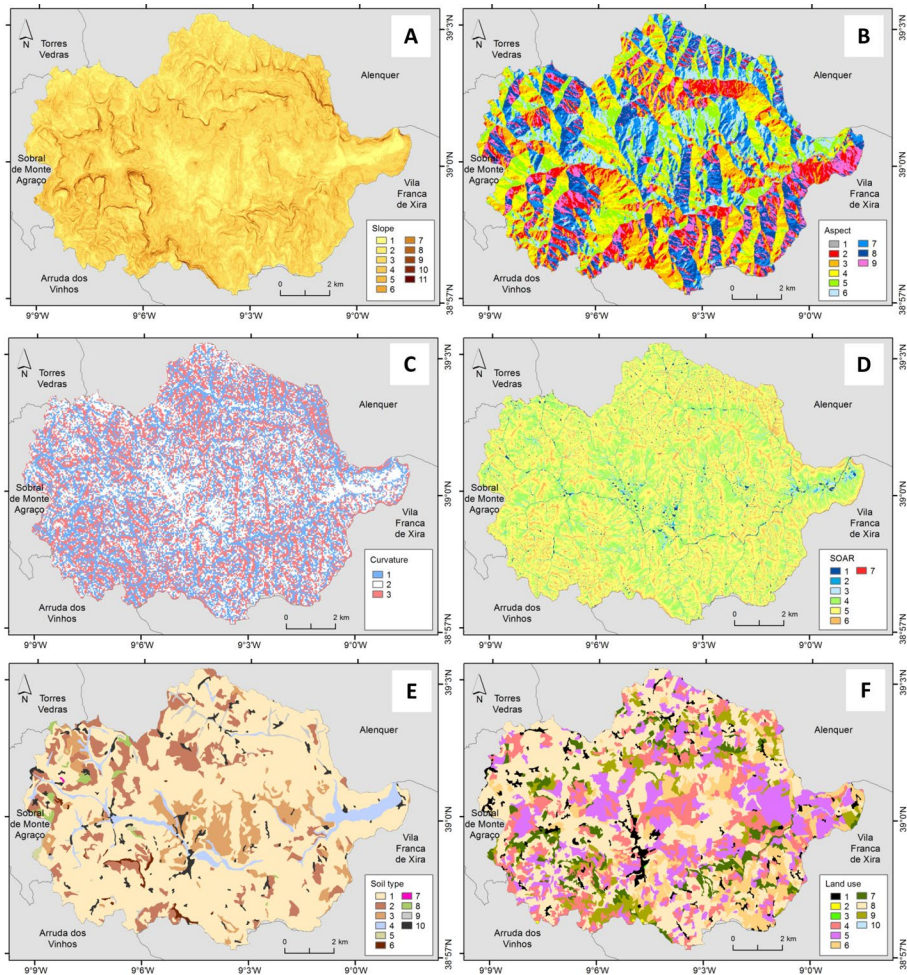
Fig. 2 Landslide predisposing factors: **A** slope angle, **B** slope aspect, **C** slope curvature, **D** slope over area ratio (SOAR), **E** soil type, and **F** land use. Lithology is presented on Fig. 1B and landslides predisposing factors classes are described in Table 3

basin. However, moderate and high slopes (> 15°) are only present in 12.5% of the study area (Fig. 2A).

2.2 Rainfall patterns and landslide occurrence

Most landslides that occurred in the north of Lisbon region since the late 1950s show a clear climatic signal and are triggered by rainfall (Zêzere et al. 1999a, b). In the study area the mean annual precipitation (MAP) is around 760 mm, with the highest concentration of rainfall observed from October to March (Zêzere et al. 2015). Until 2010, 25 rainfall-triggered landslide events were identified, mainly in rainy years with annual precipitation above the MAP (Zêzere et al. 2015; Zêzere and Trigo 2011). Similarly to other examples
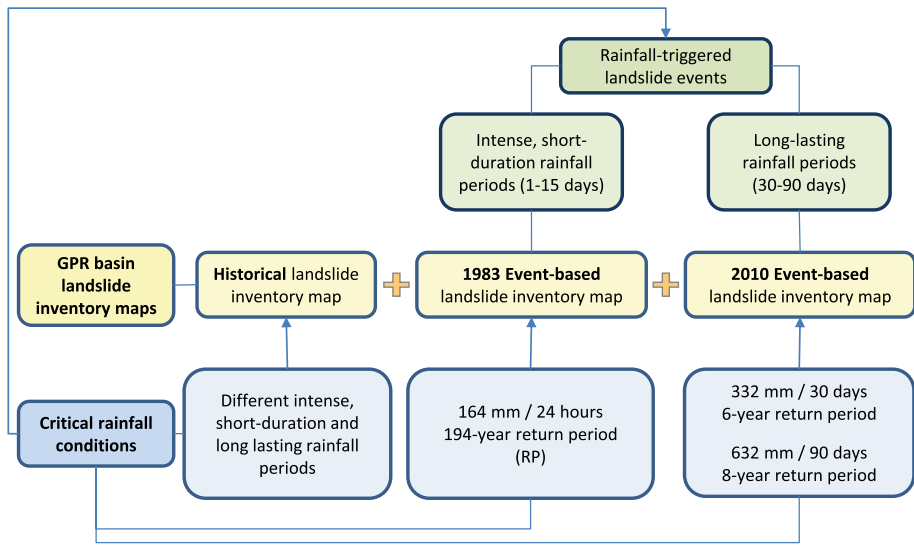
Fig. 3 Relationship between regional rainfall-triggering critical conditions and event-based landslide inventory maps

worldwide (Van Asch et al. 1999; Gostelow 1991; Iverson 2000), two main rainfall patterns (Fig. 3), associated to different rainfall critical conditions, have been recognized in the study area by using daily rainfall data as a proxy of the triggering mechanisms responsible for shallow and deep-seated landslides occurrence on natural slopes (Ferreira 1984; Zêzere et al. 1999b, 2005, 2015): (i) intense, short-duration rainfall periods (1–15 days); and (ii) long-lasting rainfall periods (30–90 days).

In the present work a landslide event is any date for which at least five individual landslides are known to have occurred on natural slopes. (Zêzere et al. 2015; Zêzere and Trigo 2011). The landslide events associated with the critical rainfall conditions described in (i) primarily occur during autumn, especially in November, as a result of polar and tropical interferences, which predominantly trigger shallow landslides. The landslide events triggered by the rainfall critical conditions described in (ii) are related to abundant and persistent winter rain, sometimes following a well-watered autumn. These conditions are frequently responsible for the triggering of larger and deeper landslides. The last landslides event type is often preceded by precipitation clustering over long temporal windows of 23–90 days (Bevacqua et al. 2021), this is, the antecedent rainfall prior to the landslide event. The long-lasting rainfall sequences, observed in the north of Lisbon region are typically of polar origin either in zonal circulation or in blocked circulation (Ferreira 1984) and are statistically associated with the 3-month negative average values of the North Atlantic Oscillation (NAO) index (Zêzere et al. 2005).

2.2.1 The 1983 intense rainfall-triggered landslide event

On 18th November 1983 (Fig. 4A), was recorded the heaviest rainfall episode of the twentieth century in the study area (Ramos et al. 2014). In the São Julião do Tojal (SJT) rain gauge (Fig. 1A), which is considered representative for the study area (Oliveira et al. 2014), a maximum absolute daily (24-h) rainfall of 164 mm was registered
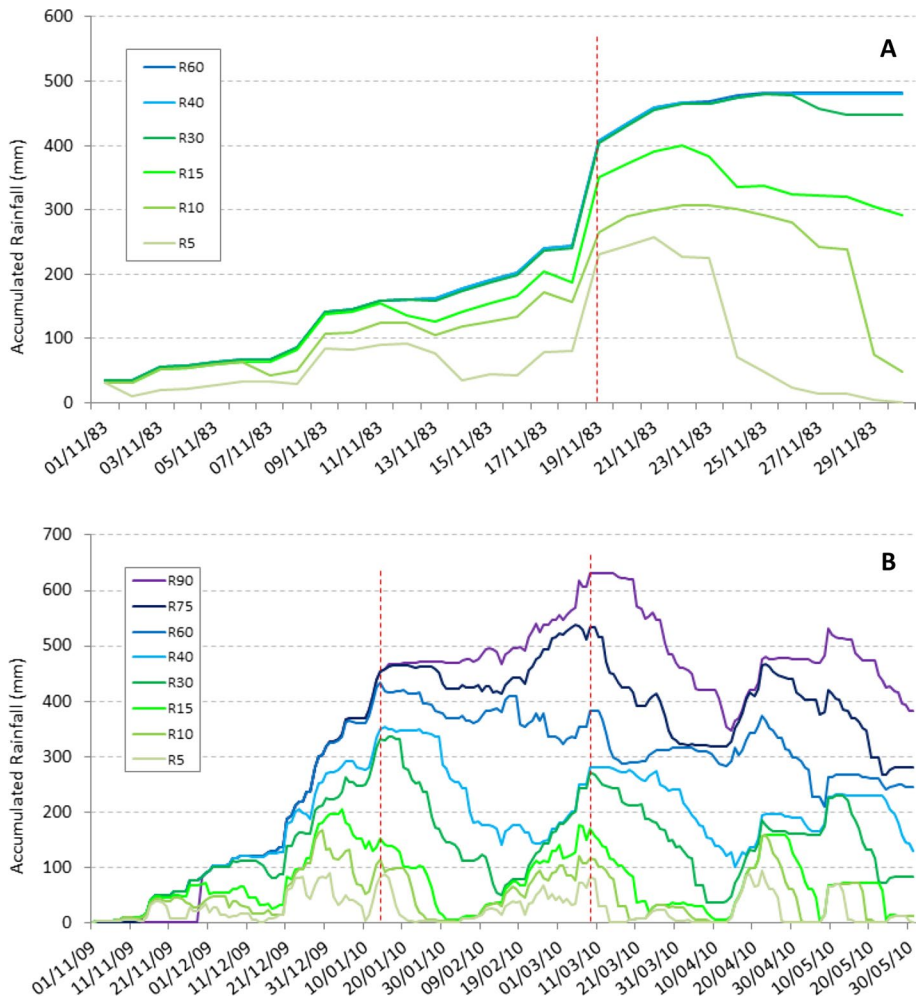
Fig. 4 Accumulated rainfall for different durations observed in SJT (Fig. 1A) related to the 1983 (**A**) and 2010 (**B**) rainfall-triggered landslide events. The dashed red line indicates the dates of the landslide events according to (Zêzere and Trigo 2011)

(Zêzere et al. 1999a, b), corresponding to a 194-year return period (RP) (Zêzere and Trigo 2011). The antecedent rainfall was not relevant for this landslide event (Zêzere et al. 1999a). The occurrence of the heavy rainfall episode was caused by an extended deep low-pressure system (990 hPa) with a frontal system extending across the Atlantic, approaching the mainland (Lisbon region) on a SW-NE trajectory (Godinho 1984). In the study area, both on the steeper natural slopes and on the anthropic cuts and fills, the rapid water infiltration triggered several shallow translational slides, due to the development of positive pore water pressure and the decrease in the material's apparent cohesion (Zêzere et al. 2015). The characteristics of the event provide a straightforward temporal identification of the rainfall event that can be related to the landslide occurrences.

2.2.2 The 2010 long lasting rainfall-triggered landslide event

In the 2009–2010 climatological year (September to August) two rainfall-triggered landslide events (Figs. 3, 4B) were documented in the north of Lisbon region (Zêzere and Trigo 2011). On 14th January, the first landslide event was recorded, which was linked to a critical rainfall of 332 mm/30 days (6-year return period). The second landslide event occurred almost 2 months later on 9th March and was associated with a critical rainfall of 632 mm/90 days (8-year return period) (Zêzere et al. 2015). During the winter period of December 2009 to March 2010, the NAO index reached its most extreme negative value since 1823. This was particularly evident from 10th December 2009 to 14th January 2010 and from 24th January 2010 to 31st March 2010 (Vicente-Serrano et al. 2011), which coincided with the dates of the landslide events. For instance, during the 4-month period, the Lisbon rain gauge (located 30 km south of the study area) recorded 958.6 mm of rainfall, which is the highest amount of rainfall ever recorded from 1865 to 2010 (Vicente-Serrano et al. 2011). The landslides triggered by this rainfall were mainly deep-seated rotational and translational slides, as reported by Oliveira (2012), Oliveira et al. (2015b), and Zêzere et al. (2015).

In the study area, the landslides were recorded from end-November to end-April, following a progressive temporal and spatial pattern in response to the daily rainfall distribution, the antecedent rainfall accumulation and the geologic/geomorphologic context (Oliveira 2012). These factors were responsible for the regional rise of the water table. In the study area landslides seem to occur during the phase of water table rise and during its high-tand (the upper soil, which is mostly unsaturated, becomes progressively saturated causing the cancellation of the negative pore pressures in a thicker portion of the soil, which contributes to destabilise the shallowest part of the slopes), and reduce their frequency when water table despite high started to lowering. Negative pore pressures are again generated in the unsaturated zone, which are favourable conditions to stability of the upper layers of the soil (Jesus et al. 2018).

According to the literature, this leads to a seasonal landslide inventory map that encompasses landslides triggered by multiple events within a singular season (Fiorucci et al. 2011). Even so, these landslides were primarily triggered by long-lasting rainfall periods (30–90 days), which clearly distinguishes them from those triggered during the 1983 rainfall event. Making an analogy with the slope progressive failure concept (Palmer and Rice 1973), we aggregated all the 2010 seasonal landslides in a single "landslide event" for modeling proposes. This assumption takes into account the progressive temporal and spatial instability that occurred in the study area during the aforementioned 5-month period of the defined 2010 landslide event, as a consequence of the progressive regional water table rise (Jesus et al. 2014, 2018). Spatially, the instability started in the SW sector of the GPR basin, mostly as shallow landslides affecting LU8 and LU7. Subsequently, in March, reached the older rocks (LU9) rich in clay minerals (almost no smectite and the expansive minerals present are chlorite and gypsum, Alonso et al. 2010) which are located in the center of the basin and lately, in the rainy period, triggered the most deep-seated landslides as a consequence of the regional groundwater table rise to position close to the topographic surface (Jesus et al. 2018; Oliveira 2012).

2.3 Historical and event-based landslide inventories

The 1983 and 2010 landslide inventory maps used in this work were based on different landslide mapping approaches that combined different techniques: detailed field mapping; high resolution aerial photo and orthophotomap interpretation; and analysis of shadow

relief models. The landslide type was defined following the classification of Cruden and Varnes (1996) and the separation between shallow and deep landslides was made considering a rupture surface depth below or above 3 m, respectively. In addition, to eliminate the potential bias in landslide susceptibility modeling due to the reduced number of debris flows and mudflows in the study area, the present work only considers landslides of the slide type that occurred on natural slopes.

2.3.1 Historical landslide inventory

The historical landslide inventory map (Fig. 1B) was based on a systematic field surveying carried out between 2006 and 2009. Landslides were mapped over orthophotomaps at the 1:2000 scale, using the drainage network and the contour lines with 5 m equidistance as ancillary information. The total number of landslides, as well as their age (absolute or relative), geometry and geolocation in the final inventory map were validated and updated by interpretation of aerial photographs and orthophotomaps, dated from 1989 to 2007, and by the identification of landslide morphometric features in a shadow relief model derived from a 1: 10,000 topographic maps. This historical landslide inventory map includes 640 landslides of the slide type occurred on natural slopes (332 deep-seated rotational slides; 210 shallow rotational slides, and 98 shallow translational slides). The landslide area (L_a) ranges from 12.4 to 262,194 m^2 (mean landslide area around 9000 m^2) and the total unstable area is 5,735,400 m^2, which corresponds to 5.2% of the GPR basin area.

2.3.2 1983 and 2010 event-based landslide inventories

Two rainfall event-based landslide inventory maps are available for the GPR basin, corresponding to the events described in Sects. 2.2.1 and 2.2.2. Both event-based landslide inventory maps were created by mapping fresh landslide features, considering the time of information acquisition.

Table 1 Number and affected area of slides included in the 1983 and 2010 rainfall event-based landslide inventories and the historical landslide inventory in the GPR basin

Landslide typology	Landslide inventory	# (%) landslides	Landslide area (L_A) (m^2)	% of study area
All slides (DRS, SRS, STS)	1983 Ev-B	173 (100)	130,750	0.12
	2010 Ev-B	162 (100)	461,309	0.42
	Historical	640 (100)	5,735,412	5.19
Deep-seated rotational slides (DRS)	1983 Ev-B	37 (21.4)	55,004	0.05
	2010 Ev-B	55 (34.0)	331,988	0.30
	Historical	332 (51.9)	5,407,044	4.89
Shallow rotational slides (SRS)	1983 Ev-B	98 (56.6)	66,411	0.06
	2010 Ev-B	74 (45.7)	114,216	0.10
	Historical	210 (32.8)	298,738	0.27
Shallow Translational slides (STS)	1983 Ev-B	38 (22.0)	9335	0.01
	2010 Ev-B	33 (20.4)	15,105	0.01
	Historical	98 (15.3)	29,631	0.03

The 1983 event-based landslide inventory map was built based on photointerpretation of black and white vertical aerial-photographs in a 1:15,000 scale, taken less than a month after the landslide event (Fig. 1B, Table 1). All landslides are temporally referenced to the 18th of November 1983. The aerial photographs georeferencing process and landslide mapping procedures were described in detail in Oliveira (2012). Visual interpretation of aerial photographs proved to be an effective technique for the detection and mapping of recent landslides, including slope failures that did not leave distinct and immediately recognizable morphological or land cover signatures (Fiorucci et al. 2011). Nowadays, recognizing the evidence of landslides that occurred over 30 years ago is virtually impossible to perform through field-based geomorphological recognition. In the study area, the landslide features tend to disappear in 10–20 years, even faster if there is an intensive agricultural activity (e.g., vineyards or cereals) or the development of activities affecting the landscape (e.g., urbanization) (Oliveira et al. 2015b). In the 1983 landslide event (Table 1), 173 slides were mapped over an area of 130,750 m^2 (0.12% of the study area). Shallow rotational slides were the dominant type (98 cases), affecting 66,411 m^2 (50.8% of the total unstable area in this event). Deep-seated rotational slides and shallow translational slides presented a similar number of cases (37 and 38, respectively), but the unstable area differed significantly. Deep-seated rotational slides were associated to 42.1% of the total unstable area during the event, while the area affected by shallow translational slides did not surpass 7%.

The inventory map of the 2010 landslide event was based on systematic field surveying performed each week from November 2009 to the end of April 2010 (Fig. 1B, Table 1). All landslides were mapped over orthophotomaps at the 1:2000 scale with contour lines (equidistance 5 m) and drainage network as ancillary information. For this event, few landslides of the slide type were mapped on natural slopes (162 cases) but the total unstable area (461,309 m^2, 0.42% of the study area) surpasses 3.5 times the unstable area associated to the 1983 landslide event. This can be explained by the occurrence of 55 deep-seated rotational slides (34% of the total number of landslides in the event) that represent 72% of the total unstable area (331,988 m^2). As in 1983, the shallow rotational slides were the most representative landslide type with 74 cases, representing 45.7% of the total number of landslides and 24.8% of the unstable area of the event. Shallow translational slides were the less represented landslide type with 20.4% (33 cases) of the total number of landslides and 3.3% of the total unstable area.

Despite the contrasting rainfall triggering conditions, both landslide events presented a similar landslide density (1983 = 1.6 landslides/km^2; 2010 = 1.5 landslides/km^2).

3 Methods

3.1 Analysis of landslides morphometric characteristics

The morphometric and typological attributes of landslides are typically heavily influenced by the geological and geomorphological conditions of the areas where slope failure occurs (Carrara et al. 1977). The morphometric characteristics of landslides were analyzed in each landslide event-based inventory were analyzed using 10 landslide parameters and 7 indices (Table 2). These characteristics relate to the morphometry (size and shape) of landslides and their spatial position along the slope, which is considered a proxy for landslide mobility (Garcia 2002; Zêzere 1997). Landslide parameters and indices were analyzed according to the landslide type, which includes: (i) simple descriptive statistical parameters as the

Table 2 Landslide morphometry, spatial position, mobility parameters and indices (adapted from Zêzere [1997]; Garcia [2002])

Variable	Description	Unit	Component
L_W	Landslide maximum width	m	Morphometry
L_L	Landslide maximum length	m	Morphometry
L_{maxE}	Maximum elevation in the landslide main scarp top	m	Position
L_{minE}	Minimum elevation in the landslide tip	m	Position
L_A	Landslide area	m^2	Morphometry
L_{top}	Distance between the landslide main scarp top and the slope top	m	Position
L_{base}	Distance between the landslide tip and the slope base	m	Position
S_L	Slope length	m	Position
L_{DAL}	Landslide depletion area maximum length	m	Morphometry
L_{DA}	Landslide depletion area	m^2	Morphometry
$I1\ (L_{top}/S_L)$	Defines how close to the slope top the landslide scarp is. Values closer to 0 indicate proximity of the landslide scarp to the slope top. Negative values indicate that the landslide scarp is located in the slope top	–	Position
$I2\ (L_{base}/S_L)$	Defines how close to the slope base the landslide tip is. I2 > 1 indicate proximity of the landslide tip to the slope base. I2 < 0 indicate that the landslide tip lies beyond the slope base (e.g., in the alluvial plain or upslope in the opposite slope)	–	Position
$I3\left(\dfrac{L_{maxE}-L_{minE}}{S_L}\right)$	It represents a landslide mobility index. I3 > 1 indicate the prevalence of a vertical fall component. I3 < 1 indicate the opposite. As negative is a value more distant is the landslide tip to the landslide scarp. This index also gives an indication of the slope gradient along the landslide area	–	Mobility
$I4\ (L_W/L_L)$	Defines the proportional relationship between the maximum landslide width and its maximum length. I4 > 1 landslides larger than long; I4 < 1 landslides longer than wide	–	Morphometry
$I5\ (\sqrt{L_A}/L_L)$	I5 is an index that reflects the landslide shape	–	Morphometry
$I6\ (L_A/L_{DA})$	The index represents the number of times that the depletion area is reduced by comparison with the total landslide area	–	Morphometry
$I7\ (L_L/L_{DAL})$	The index represents the number of times that the maximum length of the depletion area is less than the maximum length of the slope movement	–	Morphometry

mean, maximum and minimum values and standard deviation (SD); and (ii) the analysis of variance (One-way ANOVA). The morphometric parameters were measured using horizontal planimetric equivalents of real distances, considering the predominance of gentle to moderate slopes in the study area (less than 15° in 87.5% of the study area). The F-test (analysis of variance) and the level of statistical significance were computed for each landslide parameter and indices. The level of statistical significance was obtained after logarithmic normalization of data.

3.2 Landslide probability-density relationship

The relationship between the frequency of landslides and the landslide area (L_A) was evaluated using the probability-density function (*pdf*) described in Eq. (1) (Van Den Eeckhaut et al. 2007; Malamud et al. 2004).

$$pdf(L_A) = \frac{1}{L_N} \times \frac{\delta L_N}{\delta L_A} \tag{1}$$

where L_A is the landslide area; L_N is the total number of landslides; and δL_N is the number of landslides as a function of a given class amplitude δL_A, for which a class amplitude increments of 1.5 has been adopted.

3.3 Landslide susceptibility assessment and validation

A dataset of seven variables was selected as independent landslide predisposing factors (Figs. 1, 2 and Table 3): lithology, slope angle, slope aspect, slope curvature, slope over area ratio (SOAR), soil type and land use. These variables had successfully explained the relationship between landslides and the most favorable terrain conditions for landslide occurrence in the study area through the application of data-driven methods (Oliveira et al. 2015b, 2017; Zêzere et al. 2017).

The landslide susceptibility was assessed using the Information Value (IV) method (Yin and Yan 1988). The method allows to rank the susceptibility of each terrain mapped unit (pixel 5×5 m) of the study area. The IV susceptibility score obtained for each variable class, assumed as landslide predisposing factor, is based on the logarithmic normalization of the ratio between the conditional probability to find a landslide in a certain class of a predisposing factor and the a priori probability to find a landslide in the study area. The final susceptibility score for each terrain mapped unit is the sum of each partial IV score calculated for each class of each landslide predisposing factor. IV scores equal to zero indicate that the relationship between landslide occurrence and the independent variable used to discriminate stable and unstable areas is unclear. Negative IV scores indicate a favorable condition for slope stability and positive IV scores indicate a favorable condition for slope instability in the terrain unit, which will be higher as the IV score increases (Zêzere et al. 2017).

In order to evaluate the reliability of using an event-based landslide inventory map to assess landslide susceptibility at the basin scale, two modeling groups were created. Modeling Group I include eight landslide susceptibility models that compare landslide susceptibility based on the landslide type associated with the rainfall-triggered landslide events of 1983 and 2010 (Table 4). Models 1a and 1b use the complete event-based landslide inventory map, encompassing all considered landslide types; models 2a–2b, 3a–3b, and 4a–4b

Table 3 Information Value (IV) scores according to the dataset of landslide predisposing factors, landslide types and rainfall event-based landslide inventories

Thematic layers	Class ID	Study area (%)	Deep rotational slides (DRS)		Shallow rotational slides (SRS)		Shallow translational slides (STS)	
			1983	2010	1983	2010	1983	2010
Slope angle (°)								
0–2	1	33.6	−3.627	−3.699	−1.363	−4.076	−3.106	−3.391
2–5	2	31.8	−3.849	−2.956	−2.010	−4.468	−2.762	−3.495
5–10	3	5.2	−1.200	−0.079	−0.294	−0.151	−3.106	−3.194
10–15	4	17.2	0.438	**0.619**	0.150	**0.699**	0.141	−0.741
15–20	5	42.5	**1.415**	**0.588**	**1.050**	**0.566**	**1.235**	0.257
20–25	6	22.7	**1.564**	0.028	**1.129**	0.300	**1.652**	**2.063**
25–30	7	7.3	**1.267**	−0.285	**1.193**	−0.809	**2.049**	**2.857**
30–35	8	2.8	**1.084**	−0.294	**1.632**	−0.802	**2.956**	**3.330**
35–40	9	1.3	**1.076**	−0.530	**1.360**	−0.760	**3.184**	**3.783**
40–45	10	0.6	**1.952**	−1.079	0.535	−4.468	**2.690**	**2.533**
> 45	11	0.3	−5.488	−6.332	−3.154	−4.468	**1.735**	**2.389**
Aspect								
Flat	1	0.001	−5.488	−2.859	−0.839	−2.077	−3.106	−3.495
N (337.6°–22.5°)	2	5.8	0.637	0.348	**1.039**	−0.331	−0.886	0.771
NE (22.6°–67.5°)	3	16.1	**1.100**	**0.448**	**0.803**	**0.610**	**0.974**	0.120
E (67.6°–112.5°)	4	16	−1.634	−0.016	−0.342	**0.460**	−0.336	**0.963**
SE (112.6°–157.5°)	5	57.8	−2.604	−0.205	−3.154	−1.883	0.223	−0.654
S (157.6°–202.5°)	6	0.5	−5.488	0.132	−1.462	−1.270	−3.106	−3.495
SW (202.6°–247.5°)	7	0.1	−2.585	−0.531	−2.683	0.096	0.503	−3.495
W (247.6°–292.5°)	8	0.6	−0.264	−0.525	−1.571	0.155	−0.898	−0.736
NW (292.6°–337.5°)	9	34.6	0.748	−0.122	0.582	−0.242	−0.527	−0.581
Slope curvature								
Concave	1	34.6	0.297	0.124	0.261	0.072	−0.003	0.439
Straight	2	33.6	−0.290	0.186	−0.041	−0.002	−0.568	−0.904

Table 3 (continued)

Thematic layers	Class ID	Study area (%)	Deep rotational slides (DRS)		Shallow rotational slides (SRS)		Shallow translational slides (STS)	
			1983	2010	1983	2010	1983	2010
Convex	3	31.8	−0.118	−0.443	−0.330	−0.083	0.378	0.029
Slope over area ratio								
0	1	16.4	−0.732	−2.539	0.443	−2.722	−0.493	−1.343
0–0.00001	2	17.5	−2.483	−3.885	0.127	−4.468	−0.704	−3.495
0.00001–0.0001	3	11.6	−1.194	−0.845	−0.923	−2.825	−2.506	−1.341
0.0001–0.001	4	6.1	−0.525	**0.139**	−0.189	−0.189	−1.828	−0.991
0.001– 0.01	5	38.6	0.206	0.091	0.099	**0.237**	0.296	−0.108
0.01–0.1	6	6.3	0.071	−0.869	−0.081	−1.133	**0.425**	**1.362**
>0.1	7	0.1	**1.085**	−6.332	−3.154	−4.468	−3.106	**2.420**
Lithology								
Alluvium	LU1	3.1	−1.045	−2.293	0.749	−1.965	−0.652	−3.495
Limestone intercalations	LU2	0.003	−5.488	−6.332	−3.154	−4.468	−3.106	−3.495
Conglomerates, Sandstones, Mudstones	LU3	0.003	−5.488	−6.332	−3.154	−4.468	−3.106	−3.495
Sandstones, marls and limestones	LU4	0.001	−5.488	−6.332	−3.154	−4.468	−3.106	−3.495
Limestones and marls	LU5	5.8	**1.202**	−1.776	**1.673**	−0.556	**1.764**	−3.495
Mudstones, sandstones, marls and limestones	LU6	16.1	0.446	−1.887	−0.199	−0.884	−0.473	−1.063
Coralline limestones	LU7	16.0	−5.488	**0.812**	−3.154	−4.468	−3.106	−3.495
Limestones	LU8	0.5	0.185	−1.332	−0.386	−2.953	**0.470**	**1.422**
Marls, clays and sandstones	LU9	57.8	−0.554	**0.454**	−0.406	**0.392**	−0.725	−0.717
Conglomerates	LU10	0.1	−5.488	−6.332	−3.154	−4.468	−3.106	−3.495
Dykes and magmatic intrusions	LU11	0.6	**1.284**	−6.332	−2.715	**1.738**	0.643	−3.495
Soil type								
Cambisols	1	1.3	**0.202**	**0.186**	0.101	**0.105**	0.121	−0.104

Table 3 (continued)

Thematic layers	Class ID	Study area (%)	Deep rotational slides (DRS)		Shallow rotational slides (SRS)		Shallow translational slides (STS)	
			1983	2010	1983	2010	1983	2010
Luvisols	2	1.1	−1.494	−0.964	−0.009	−1.801	−0.931	0.115
Vertisols	3	3.3	−0.821	**0.179**	−1.800	**0.833**	−3.106	−2.246
Fluvisols	4	25.3	−1.158	−6.332	0.293	−3.876	0.145	−3.495
Kastanozems	5	59.8	−5.488	−6.332	−3.154	−4.468	−3.106	−3.495
Rock outcrops	6	9.1	**1.255**	−6.332	−3.154	−4.468	**2.366**	**3.737**
Litosols	7	0.03	−5.488	−6.332	−3.154	−4.468	−3.106	−3.495
Cambisols (lhitolic)	8	71.3	−5.488	−2.676	−3.154	−4.468	−3.106	−3.495
Colluvium	9	11	**1.271**	−6.332	**0.920**	−4.468	**1.567**	−3.495
Social areas	10	8.2	−5.488	−6.332	−1.261	−4.468	−3.106	−3.495
Land use								
Urban areas	1	4.2	−1.371	−6.332	−3.154	−2.488	−3.106	−0.784
Quarry	2	0.3	−5.488	−6.332	−3.154	−4.468	−3.106	−3.495
Urban green spaces	3	0.5	−5.488	−6.332	−3.154	−4.468	−3.106	−3.495
Cultivated areas	4	0.02	**0.520**	0.060	**0.501**	0.019	0.662	−3.446
Vineyard	5	0.8	−0.641	**0.621**	0.055	**0.562**	−0.451	−0.920
Fruit trees	6	1	−0.650	0.008	−0.614	−0.340	−1.807	−0.732
Forest	7	2.7	**0.744**	−0.314	−0.292	−0.110	**1.141**	**1.624**
Heterogeneous cultivated areas	8	3.4	−0.154	−0.585	−0.306	−0.227	−0.380	−0.805
Shrubs and herbaceous vegetation	9	0.03	**0.500**	**0.678**	**0.882**	**0.216**	**0.438**	**1.776**
Water	10	0.01	−5.488	−6.332	−3.154	−0.340	−3.106	−3.495

Higher scores are highlighted is bold

use, respectively, the event-based deep-seated rotational slides, shallow rotational slides and shallow translational slides (Table 4). Modeling Group II aims to identify the similarities/differences between the historical landslide susceptibility model and the event-based landslide susceptibility models. The Modeling Group II includes four landslide susceptibility models (models 5a–5d) computed to assess the predictive capacity of the historical landslide susceptibility map when validated with independent event-based landslide inventories (Table 4) and vice versa.

The landslide susceptibility model's adjustment and independent predictive capability were assessed by computing the respective Receiver Operating Characteristic curves (ROC) and by calculating the Area Under the Curve of the Receiver Operating Characteristic curve (AUC-ROC) values according to the training and validation scheme defined in Table 4. The AUC-ROC is a commonly used measure of the discriminative capacity of a classification model and uses both the landslide and non-landslide terrain units to evaluate model performance. A model is considered to discriminate better than chance if the AUC is greater than 0.5, where a value of 1 is associated with a model with perfect discrimination (Jiménez-Valverde 2012; Zêzere et al. 2017).

3.4 Evaluation of the spatial agreement between landslide susceptibility maps

The study assessed the spatial agreement between landslide susceptibility maps of Modeling Group I. Four pairs of landslide susceptibility maps were grouped by landslide type for both event-based landslide inventory maps (e.g., model 1a X model 1b, Table 4). Modeling Group II produced only one historical landslide susceptibility map and no spatial comparison was made. Firstly, the nine landslide susceptibility maps listed in Table 4 (under the Training Group column) were classified into 10 susceptibility classes using the quantile classification method. This classification ensures that each susceptibility class in all maps contains the same 10% of grid cells within the study area, allowing for a relative comparison (Oliveira et al. 2017). The classification procedure was solely used to assess the spatial agreement between the pair of maps. This was done using the Map Comparison Kit tool (Visser and Nijs 2006) on a cell-by-cell basis. The resulting contingency tables, Kappa statistics (Kappa Index, Kappa histogram, and Kappa location) and the fraction of terrain units equally classified in each pair of landslide susceptibility maps were used to evaluate susceptibility classification dispersion and spatial agreement among pairs of equivalent landslide susceptibility maps.

4 Results

4.1 Statistical properties of the 1983 and 2010 landslide events inventories

The main differences between the 1983 and the 2010 landslide events, regarding the number and type of landslides were described in Sect. 2.3.2. Despite the similar number of landslide cases and the predominance of shallow rotational slides in both landslide events, a 12.6% increase in the number of the deep-seated rotational slides was verified in the 2010 event, contrasting with a 10.9% increment in the number of shallow rotational slides in the 1983 event (Fig. 5A). These results are consistent with the predominant landslide types expected to occur in the region in response to critical conditions of prolonged or short-lived intense rainfall (Zêzere et al. 2015). They are further supported by the statistical

Table 4 Landslide susceptibility modelling strategy: training and validation groups

Modelling strategy	Model #	Landslide inventories		
		Training group	Validation group (model adjustment)	Validation group (independent validation)
Modelling group I	1a	1983 Ev-B	1983 Ev-B	2010 Ev-B
	1b	2010 Ev-B	2010 Ev-B	1983 Ev-B
	2a	1983 DRS	1983 DRS	2010 DRS
	2b	2010 DRS	2010 DRS	1983 DRS
	3a	1983 SRS	1983 SRS	2010 SRS
	3b	2010 SRS	2010 SRS	1983 SRS
	4a	1983 STS	1983 STS	2010 STS
	4b	2010 STS	2010 STS	1983 STS
Modelling group II	5a	Historical	Historical	1983 Ev-B
	5b	Historical (=5a)	Historical (=5a)	2010 Ev-B
	5c	1983 Ev-B (=1a)	1983 Ev-B (=1a)	Historical
	5d	2010 Ev-B (=1b)	2010 Ev-B (=1b)	Historical

analysis of the landslide morphometric attributes for the 1983 and 2010 landslide events (Table 5). Although we are aware that for some landslide types, the number of landslides is too low, it should be noted that for many morphometric attributes and indices there are no significant differences between landslides included in the two event-based inventories, as it is showed by the F-test values and the statistical significance levels below 95% (ns—not significant) (Table 5). Shallow translational slides have virtually equivalent morphometric characteristics in both event-based landslide inventories.

The main differences between landslide inventories are related to the specific landslide size parameters (L_L, L_W and L_A) and the maximum and minimum elevations of landslide types DRS and SRS (Fig. 5B–D), where the variance reaches significance levels of 0.01 (99%). The deep-seated and shallow rotational slides triggered during the 2010 landslide event present a larger width and length, which was reflected in a wider unstable area. In the 2010 landslide event, larger DRS occurred mostly at lower elevations compared to the corresponding DRS occurred during the 1983 landslide event, which are typically smaller in size.

4.2 Landslide probability-density relationship

The landslide distribution as a result of a probability-density function (Fig. 6A) can be used to better characterize the landslide hazard in the study area, by extracting the probability of landslide occurrence given a certain magnitude scenario (landslide size) (Fig. 6B). Based on the historical landslide inventory, 70% of the new slides that are expected to occur in the GPR basin will have an area under 6000–7000 m^2 (L_A½ ± 77.5 m to 83.7 m, respectively) (Fig. 6B). In an undetermined future time span, 20% of the larger slides will have an area above 10,000 m^2, i.e., L_A½ ± 100 m. The probability of landslide occurrence tends to decrease significantly for slides larger than 10,000–20,000 m^2 and landslides larger than 100,000 m^2 (L_A½ ± 316.2 m) have a very low probability of occurrence (less than 1%).

In addition, landslides smaller than 100 m^2 have a slightly higher probability of occurrence in the historical inventory when compared to the 1983 and 2010 event-based landslide inventories. Moreover, it is noticed the progressive detachment to the right side of the historical landslide inventory probability distribution curve in Fig. 6B. This is evident for landslide magnitudes greater than $L_A > 100$–200 m^2, indicating the potential for the occurrence of landslide events more severe than those registered in 1983 and 2010. The huge differences in the dependence relationship between landslide frequency and landslide area, when event-based landslide inventory maps are compared (assuming the completeness of the event-based landslide maps) are related to the short-intense or long-lasting rainfall critical conditions. Landslides from the 2010 landslide event increase in size and frequency in comparison with the 1983 landslide event.

4.3 Event-based landslide susceptibility models

The results of the eight landslide susceptibility models performed for each landslide type and for each landslide event (1983 and 2010) (cf. Sect. 3.2, models 1a–4b, Table 4) are shown in Fig. 7.

Different spatial susceptibility patterns are recognized for rotational slides (Fig. 7C–E), reflecting the spatial distribution of shallow and deep-seated rotational slides within the 1983 and 2010 landslide events. Concerning the 2010 event-based inventory maps (Fig. 7D and F), the most susceptible areas for shallow and deep-seated rotational slides occurrence are mainly concentrated where LU 9 (marls, mudstones and sandstones) outcrops, i.e., along the central and eastern part of the study area. On contrary, areas classified as more susceptible to shallow and deep rotational slides in models built with the 1983 event-based landslide inventory are more scattered in the LU9 and are concentrated in the southwestern sector of the study area where the LU5 outcrops (limestones and marls).
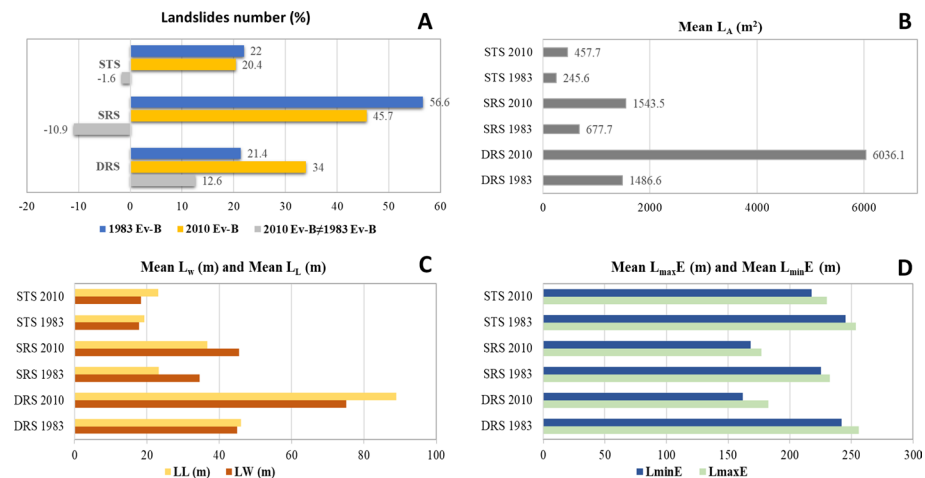

Fig. 5 Mean statistical morphometric attributes considering landslide types within the 1983 and 2010 rainfall event-based landslide inventories: **A** relative landslide number; **B** mean landslide area (L_A); **C** landslide maximum width (L_W) and landslide maximum length (L_L); and **D** maximum elevation in the landslide main scarp top (LmaxE, mean values) and minimum elevation in the landslide tip (LminE, mean values)

Table 5 Statistical parameters and analysis of variance (one way ANOVA) of landslide morphometric attributes and indexes considering landslide types within the 1983 and 2010 rainfall event-based landslide inventories. F – variance F-tests results and corresponding significance levels; $p < 0.01$—significance level higher than 99%; $p < 0,05$—significance level higher than 95%; n.s.—not statistically significant

Landslide/slope morphometric parameters	Landslide events (# slides)	Deep rotational slides (DRS)			Shallow rotational slides (SRS)			Shallow translational slides (STS)		
		1983 (37 cases)	2010 (55 cases)	F	1983 (98 cases)	2010 (74 cases)	F	1983 (38 cases)	2010 (33 cases)	F
L_W (m)	Mean	45	75.1		34.6	45.5		17.8	18.3	
	SD	16.9	38.3	27.6	24.4	28.8	7.9	10.2	20.1	0.8
	Maximum	79	196	(0.01 < p < 0.05)	158	149	(p < 0.01)	53	98	(n.s.)
	Minimum	16	31		9	5		5	2	
L_L (m)	Mean	46	88.9		23.3	36.7		19.3	23.2	
	SD	21	68.3	20.8	19.4	31.1	17.3	9.3	15.1	1.7
	Maximum	119	442	(p < 0.01)	177	190	(p < 0.01)	49	83	(n.s.)
	Minimum	17	18		5	8		5	7	
L_{maxE} (m)	Mean	256.1	182.5		232.3	177		253.5	230	
	SD	83.6	72	10.3	83.5	75	12.9	58.6	72.8	2.4
	Maximum	369.4	348.9	(p < 0.01)	351.6	367	(p < 0.01)	335.8	355.8	(n.s.)
	Minimum	43.4	29.4		28.2	14		70	55	
L_{minE} (m)	Mean	242	161.9		225.2	168.3		245.4	217.9	
	SD	82.3	71.7	12.1	83	75.8	14.2	57.7	71	3.2
	Maximum	358.4	333.9	(p < 0.01)	347.1	358	(p < 0.01)	332	347.5	(n.s.)
	Minimum	28.9	16.4		27.2	13.5		68.8	49.5	
L_A (m^2)	Mean	1486.6	6036.1		677.7	1543.5		245.6	457.7	
	SD	933.3	8715.7	34.5	1248.8	2140.0	19.7	230.3	942.5	0.69
	Maximum	4534.6	57,851.0	(p < 0.01)	10,827.1	14,720.3	(p < 0.01)	1186.9	4976.1	(n.s.)
	Minimum	298.3	456.9		46.2	33.9		45	45.1	

Table 5 (continued)

Landslide/slope morphometric parameters	Landslide events (# slides)	Deep rotational slides (DRS)			Shallow rotational slides (SRS)			Shallow translational slides (STS)		
		1983 (37 cases)	2010 (55 cases)	F	1983 (98 cases)	2010 (74 cases)	F	1983 (38 cases)	2010 (33 cases)	F
L_{top} (m)	Mean	111.1	176.4		149.2	208.6		124.4	100.9	
	SD	130	224.2	1.4	188.9	190.6	3.8	175.1	114	0.82
	Maximum	618	1100.0	(n.s.)	938	1102.0	(n.s.)	724	500	(n.s.)
	Minimum	-4	-7		-9	-13		-7	-1	
L_{base} (m)	Mean	250.7	296.7		209	287.1		246.4	371.7	
	SD	235.9	309	1	234	272.6	1	264	359.5	3.7
	Maximum	770	1342	(n.s.)	1135.0	1288.0	(n.s.)	949	1412.0	(n.s.)
	Minimum	-11	0		-4	0		0	0	
S_L (m)	Mean	407.7	562		381.4	532.4		390.1	495.8	
	SD	241.5	396.7	4	260.4	358.2	7.3	264.8	392.5	0.94
	Maximum	940	1870.0	$(0.01 < \rho < 0.05)$	1154.0	1815.0	$(\rho < 0.01)$	1027.0	1870.0	(n.s.)
	Minimum	59	80		10	10		5	7	
L_{DAL} (m)	Mean	18.5	35.1		9.3	15.3		8.8	11.7	
	SD	11.2	26	25.1	7.5	12.4	23.7	4.2	7.3	3.9
	Maximum	69	173	$(\rho < 0.01)$	69	73	$(\rho < 0.01)$	20	35	(n.s.)
	Minimum	7	10		3	3		2	3	
L_{DA} (m²)	Mean	563.6	2356.0		246.8	584		105.9	234.4	
	SD	356.3	3512.4	38.2	394	716	23.5	88.8	517.5	1.3
	Maximum	1553.2	23,591.2	$(\rho < 0.01)$	3419.7	3658.1	$(\rho < 0.01)$	449.6	2647.0	(n.s.)
	Minimum	133.1	273.4		17.5	15.4		18.4	15.8	

Table 5 (continued)

Landslide/slope morphometric parameters	Landslide events (# slides)	Deep rotational slides (DRS)			Shallow rotational slides (SRS)			Shallow translational slides (STS)		
		1983 (37 cases)	2010 (55 cases)	F	1983 (98 cases)	2010 (74 cases)	F	1983 (38 cases)	2010 (33 cases)	F
I1 (L_{top}/S_L)	Mean	0.3	0.29		0.39	0.38		0.35	0.25	
	SD	0.28	0.26	0.2	0.34	0.26	0.45	0.33	0.22	0.11
	Maximum	0.95	0.95	(n.s.)	0.99	0.88	(n.s.)	0.94	0.89	(n.s.)
	Minimum	0	−0.04		−0.9	−0.17		−0.01	0	
I2 (L_{base}/S_L)	Mean	0.52	0.5		0.5	0.5		0.55	0.66	
	SD	0.32	0.26	0.002	0.32	0.28	3.4	0.34	0.25	3.03
	Maximum	0.95	0.97	(n.s.)	0.98	1	(n.s.)	0.98	0.98	(n.s.)
	Minimum	−0.03	0		−0.02	0		0	0	
I3 ($L_{maxE}-L_{minE}/S_L$)	Mean	0.32	0.25		0.33	0.26		0.41	0.53	
	SD	0.11	0.08	12.6	0.15	0.09	6.6	0.17	0.21	8.16
	Maximum	0.57	0.5	($\rho<0.01$)	0.67	0.58	($0.01<\rho<0.05$)	0.79	1.25	($\rho<0.01$)
	Minimum	0.19	0.11		0.07	0.06		0.18	0.22	
I4 (L_W/L_L)	Mean	1.1	1.04		1.81	1.51		1.23	0.79	
	SD	0.49	0.49	0.3	1.24	0.85	1.5	1.22	0.44	3.08
	Maximum	2.33	2.22	(n.s.)	7.15	4.42	(n.s.)	7.2	2.07	(n.s.)
	Minimum	0.26	0.38		0.3	0.34		0.21	0.1	
I5 ($\sqrt{L_A/L_L}$)	Mean	0.84	0.85		1.08	1.03		0.86	0.76	
	SD	0.19	0.21	0.01	0.36	0.3	0.39	0.38	0.19	0.89
	Maximum	1.24	1.34	(n.s.)	2.25	1.94	(n.s.)	2.47	1.29	(n.s.)
	Minimum	0.41	0.51		0.45	0.54		0.39	0.45	

Table 5 (continued)

Landslide/slope morphometric parameters	Landslide events (# slides)	Deep rotational slides (DRS)			Shallow rotational slides (SRS)			Shallow translational slides (STS)		
		1983 (37 cases)	2010 (55 cases)	F	1983 (98 cases)	2010 (74 cases)	F	1983 (38 cases)	2010 (33 cases)	F
I6 (L_A/L_{DA})	Mean	2.72	2.67		2.7	2.59		2.29	2.17	
	SD	0.78	0.76	0.15	0.75	0.64	0.98	0.58	0.61	1.04
	Maximum	5	4.85	(n.s.)	5.2	5.21	(n.s.)	4.28	4.7	(n.s.)
	Minimum	1.58	1.26		1.25	1.52		1.35	1.3	
I7 (L_L/L_{DAL})	Mean	2.66	2.56		2.52	2.41		2.26	2.03	
	SD	0.68	0.67	0.53	0.65	0.51	0.94	0.68	0.4	2.7
	Maximum	4.67	4.55	(n.s.)	4.38	4.08	(n.s.)	5	3.13	(n.s.)
	Minimum	1.69	1.25		1.5	1.25		1.44	1.33	

Regarding the shallow translational slides, the landslide susceptibility patterns are more similar (Fig. 7G and H), which is in line with the morphometric characteristics found for this type of landslides within the 1983 and 2010 landslide inventories (cf. Sect. 4.1). The most susceptible areas correspond to LU7, LU6 and LU5, which are heterogeneous in nature (limestone, marls, mudstones, sandstones and conglomerates). These lithological units comprise steep slopes and are less used for agriculture. In these locations, landslide boundaries are preserved for a longer time compared to shallow slides that occurred in agricultural areas like those occupied by LU9.

The different spatial susceptibility pattern associated to the 1983 and 2010 landslide events is also evident in models built with the overall number of landslides (Fig. 7A and B), which reflects the dominance of rotational slides, in number and size, in both event-based inventories.

Table 3 summarizes the predisposing factors classes and the Information Value scores obtained for the landslide susceptibility models built with different landslide types within the 1983 and 2010 event-based landslide inventories. The most favorable terrain conditions for the occurrence of deep-seated and shallow rotational slides are different in the study area, depending on the hydrological conditions associated to each landslide event. The most favorable conditions for the 1983 landslide event were the following: N and NE facing slopes; slopes ranging from 15° to 45°; SOAR higher than 0.1; the presence of LU5 (limestone and marls) and LU11 (dykes and magmatic intrusions); the presence of rock outcrops or colluvium as soil types; and the presence of cultivated areas, forest or shrubs and herbaceous vegetation. For the 2010 landslide event, the most favorable conditions were the following: N, NE and E facing slopes; slopes ranging from 10° to 20°; SOAR ranging from 0.0001 to 0.01; the presence of LU7 (coralline limestone), LU9 (marls, mudstones and sandstones) and LU11 (dykes and magmatic intrusions); the presence of cambissols and vertissols; the presence of vineyards or shrubs and herbaceous vegetation. Considering the shallow translational slides, prone areas are similar for both susceptibility models built with the 1983 and 2010 landslide events: slopes higher than 20° (which corresponds to areas with less agricultural activities); areas with little water accumulation (i.e., with high values of SOAR); the presence of forest or shrubs and herbaceous vegetation; the presence of rock outcrops and colluvium deposits.

Table 6 summarizes the spatial agreement registered in each pair of landslide susceptibility maps, considering the landslide type. The results highlight the low spatial agreement between the 1983 and the 2010 event-based landslide susceptibility maps, even when comparing each landslide type individually. The spatial disagreement between models is also clear in Table 7, which summarizes the Kappa statistic values resulting from the comparison of classified landslide susceptibility maps built with the 1983 and 2010 event-based landslide inventories. The spatial agreement is higher for shallow translational slides susceptibility maps (Kappa index = 0.127; fraction equally classified = 21%), potentially confirming the significant similarity in landslide predisposing conditions belonging to this category in both event-based landslide inventories.

The validation of the eight landslide susceptibility models (Fig. 7A–H) is assessed using the ROC curves and the AUC-ROC values, summarized in Fig. 8A (for models based on the 1983 rainfall event-based landslide inventory) and Fig. 8B (for models based on the 2010 rainfall event-based landslide inventory). In both cases, there is a good adjustment of the models when the landslide susceptibility map is cross tabulated with the same landslides used to construct the model (filled lines in Fig. 8A and B). The AUC-ROC values of the model adjustment built with the 1983 (Fig. 8A) and the 2010 (Fig. 8B) event-based
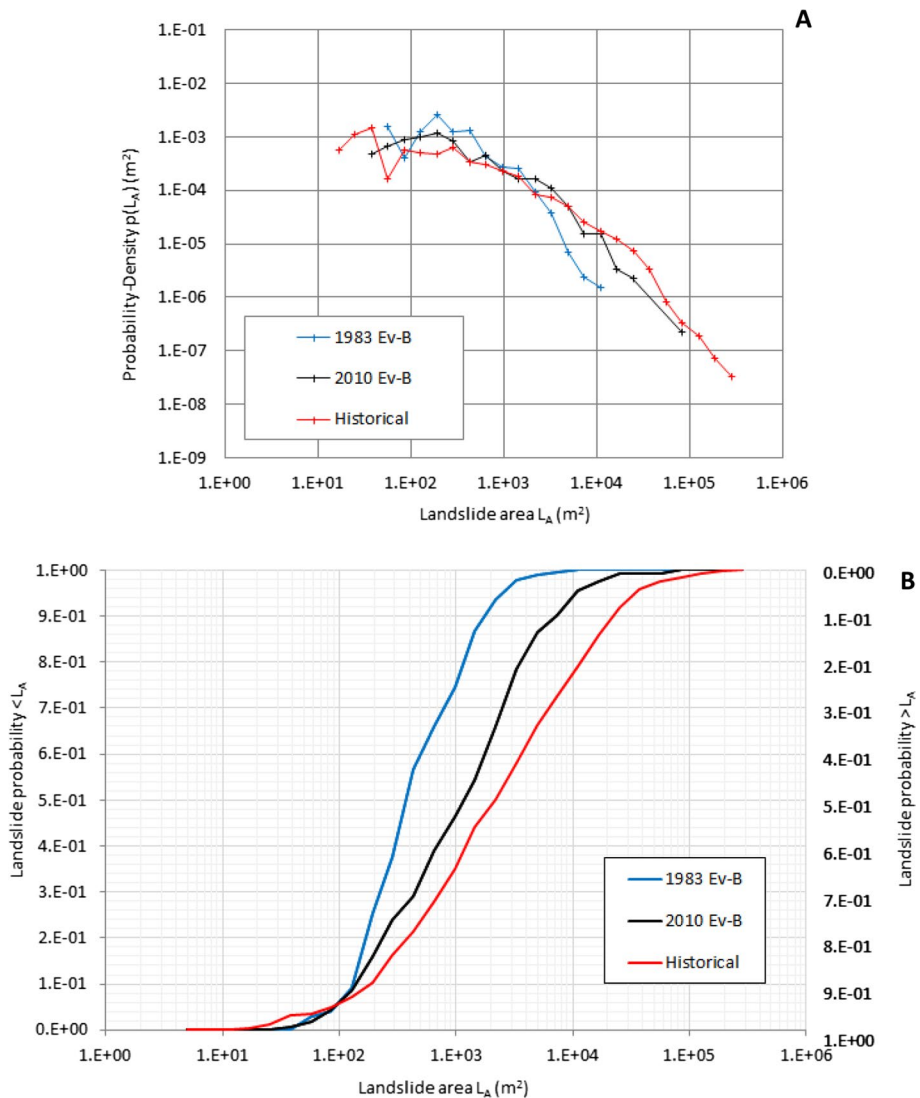
Fig. 6 Landslide probability density distribution on landslide area (L_A): **A** and probability of landslide magnitude (L_A); **B** for 1983 and 2010 rainfall event-based landslide inventories and for the historical landslide inventory. Ev-B = Event-Based

landslide inventory ranges between 0.884–0.922 and 0.811–0.959, respectively, showing a high goodness of fit of landslide susceptibility models.

On the contrary, the capacity of susceptibility models to correctly predict landslides pertaining to a landslide inventory different from the one used to build the model is typically modest, as it is attested by AUC-ROC of dashed curves in Fig. 8A and B. These AUC-ROC values for the total set of susceptibility models built with rotational slides (models 2a, 2b, 3a, 3b), as well as for susceptibility models built with the total landslide inventories (models 1a and 1b) do not surpass 0.635. The exception is found in susceptibility models

built with shallow translational slides, since the model based on landslides occurred in 1983 (model 4a) is highly effective in predicting shallow translational slides that occurred in 2010 (AUC-ROC=0.920). However, the capacity of the model based on the 2010 event (model 4b) to predict the location of shallow translational slides occurred in 1983 is significantly lower (AUC-ROC=0.713). The results indicate that relying solely on event-based landslide inventories to model landslide susceptibility is inadequate. This is due in part to the fact that landslides of the same type can be triggered by different critical rainfall conditions, which are in turn associated with different terrain predisposing conditions.

4.4 Landslide susceptibility model based on the historical landslide inventory

The next step was to evaluate to what extent a landslide susceptibility model based on a historical landslide inventory can be validated using these event-based landslide inventory maps. A new landslide susceptibility model was constructed using the historical landslide inventory for training purposes (models 5a and 5b). The landslide susceptibility map based on the historical inventory is shown in Fig. 9. Additionally, the susceptibility model based on the historical landslide inventory map was independently validated with the event-based landslide inventories not used for training, i.e., the inventory 1983 Ev-B (model 5a) and the inventory 2010 Ev-B (model 5b). The inverse modeling approach was also performed, which means using each of the event-based landslide inventories for training and the historical landslide inventory for validation (models 5c and 5d). Figure 10 presents the ROC curves and AUC-ROC values for these models. The historical landslide susceptibility model is not effective in predicting the 1983 landslide event (AUC-ROC=0.57), but it performs well in predicting the 2010 landslide event (AUC-ROC=0.73).

These results are consistent with the AUC-ROC obtained for the inverse models, which show the higher capacity of susceptibility model built with the 2010 landslide event to correctly predict the spatial location of landslides included in the historical inventory (AUC-ROC=0.72 against 0.59 for model built with the 1983 landslide event). Moreover, the AUC-ROC values obtained for models 5b and 5d are not far from the goodness of fit of the landslide susceptibility model based on the historical inventory (red curve in Fig. 10, AUC=0.79). Therefore, the 2010 event-based landslide inventory proved to be the most similar to the historical landslide inventory.

5 Discussion: advantages and limitations

5.1 How representative is an event-based landslide inventory map of the total landslide activity and distribution in a study area?

Two main differences were observed in the geometry and spatial distribution of landslides within the GPR basin in relation to the event-based landslide inventory maps: (i) despite a similar number of landslides in both rainfall-triggering events, the total unstable area registered during the 2010 event was nearly four times higher than that in 1983 event. We also acknowledge that the use of a seasonal inventory for 2010 introduces some bias in this respect.

The hydrological settings for the occurrence of deep-seated slow-moving landslides are normally related to pore water pressure accretion, requiring cumulative rainfall events to

Fig. 7 Landslide susceptibility maps modelled with the 1983 and 2010 rainfall event-based landslide ▶ inventories considering different landslide types: **A** 1983 event-based landslide inventory (Model 1a, 1983 Ev-B); **B** 2010 event-based landslide inventory (Model 1b, 2010 Ev-B); **C** 1983 deep rotational slides (Model 2a, 1983 DRS); **D** 2010 deep rotational slides (Model 2b, 2010 DRS); **E** 1983 shallow rotational slides (Model 3a, 1983 SRS); **F** 2010 shallow rotational slides (Model 3b, 2010 SRS); **G** 1983 shallow translational slides (Model 4a, 1983 STS); and **H** 2010 shallow translational slides (Model 4b, 2010 STS)

trigger a slope failure (Sidle and Bogaard 2016). In the study area, and in relation to the 2010 landslide event, evidences were found linking the first occurrence or successive reactivations of deep-seated and larger rotational slides (DRS) in LU9 (Fig. 1) to the regional rise of the water table to positions closer to or above the topographic surface (Jesus et al. 2018). In addition, significant suction changes resulting from drying after heavy rainfall periods are one of the main causes of rock physical disaggregation in evolutive materials such as LU9 marls. This process promotes the degradation of the marls mechanical properties, such as strength, cohesion and stiffness, leading to intensified water infiltration, weathering and a reduction of the sliding shear strength (Alonso et al. 2010). In the study area, the thickness of the weathered zone ranges from 0.5 to 5 m, with the materials in situ being saturated independently of the depth and degree of weathering (Alonso et al. 2010). These values agree with the deeper positions of the rupture surfaces of the deep-seated and larger rotational slides.

For the 2010 landslide event, a good regional adjustment was also found between shallow landslide occurrence and fluctuations of water table levels in LU9. This relation was found to be less sensitive in LU5, LU6 and LU7 (Jesus et al. 2018). Finally, Jesus et al. (2018) pointed out, as a possible cause, the stratigraphic sequence which led to differences in vertical permeability and to the development of perched water tables and/or confinement of local aquifers beds, being both not captured by the regional hydrological model used to relate water table position over those lithological units.

Rotational slides registered during the 1983 landslide event are less in number and small in area and occurred at higher slopes (from 15° to 45°). The hydrological mechanism that triggered these landslides was certainly associated with the sudden infiltration of water into the soil, thus developing a wetting front. The minimal influence of water table fluctuations on slope instability agrees with the low cumulative antecedent rainfall registered prior to the event day. Therefore, this event depended almost exclusively on the 24-h rainfall, whose distribution was not uniform along the study area (Fig. 11). The rainfall amount was higher in the west part of the RGP basin, which partially explains the observed concentration of landslides on that part of the basin.

In the GPR basin there are significant differences regarding the dependence relationship between landslide frequency and landslide area, whether the event-based landslide inventory maps related to short-intense (1983) or long-lasting rainfall critical conditions (2010) are compared. Landslides increase in size and frequency when triggered by long-lasting rainfall critical conditions. We acknowledge that having only one inventory per precipitation pattern may not be representative of all critical precipitation conditions that have triggered landslide events in the past. However, these event-based landslide inventory maps are related to the some of the most rainfall critical conditions occurred in the study area. In the 1983 event are related to the heaviest rainfall event over the twentieth century (Ramos et al. 2014) and in the 2010 seasonal "landslide event" to the maximum rainfall value recorded from 1865 to 2010 (Vicente-Serrano et al. 2011). Therefore, we assume that they are to some extent representative of the contrasting critical rainfall conditions that generate landslides in the study area.
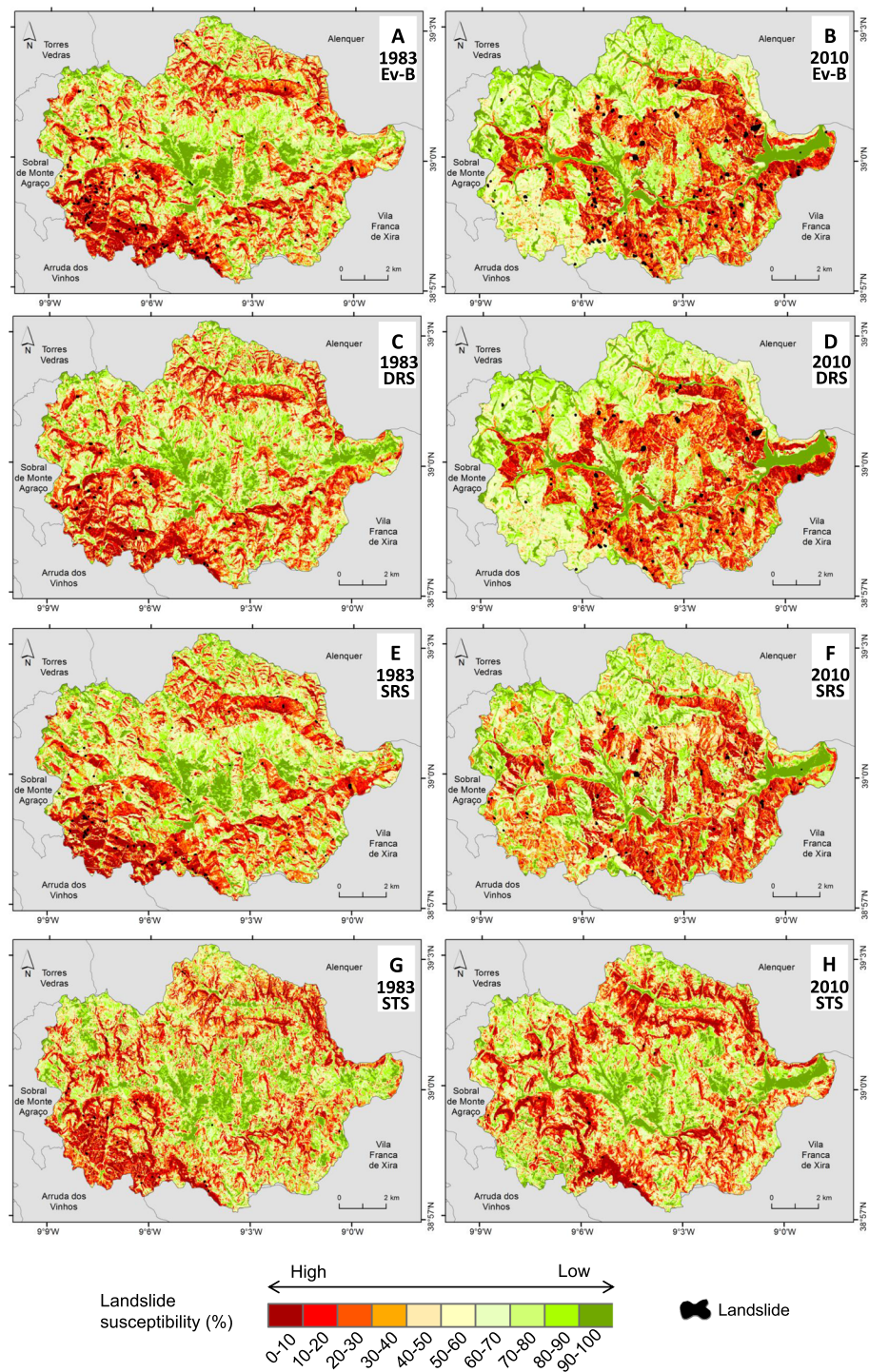
Landslide susceptibility (%)

High ← → Low

0-10 10-20 20-30 30-40 40-50 50-60 60-70 70-80 80-90 90-100

Landslide

Table 6 Contingence tables extracted from the overlay between the 1983 and 2010 rainfall event-based landslide susceptibility maps considering the landslide types

Map 1 (1983) \ Map 2 (2010)	0–10	10–20	20–30	30–40	40–50	50–60	60–70	70–80	80–90	90–100	Σ Map 1
Event-based landslide inventory (Ev-B)											
0–10	**1.70**	0.85	0.82	1.13	2.00	1.96	0.87	0.19	0.25	0.18	9.93
10–20	1.97	**1.52**	1.08	0.76	0.91	1.82	1.12	0.32	0.27	0.17	9.95
20–30	1.81	1.32	**1.31**	0.90	0.79	1.62	1.08	0.58	0.31	0.21	9.94
30–40	1.43	1.44	1.47	**1.11**	0.94	1.14	0.97	0.76	0.48	0.26	10.01
40–50	0.83	1.35	1.27	1.23	**0.83**	1.09	1.39	0.72	0.81	0.49	10.00
50–60	1.01	0.89	0.85	1.38	1.07	**0.82**	1.11	0.89	1.20	0.74	9.97
60–70	0.75	0.95	1.07	1.27	1.03	0.50	**1.20**	1.20	1.15	0.86	9.97
70–80	0.16	1.06	1.36	1.15	1.52	0.53	0.80	**0.94**	1.49	1.04	10.05
80–90	0.08	0.39	0.78	1.08	0.87	0.34	0.65	1.47	**2.23**	2.25	10.14
90–100	0.04	0.08	0.07	0.12	0.10	0.17	0.90	2.93	1.81	**3.81**	10.02
Σ Map 2	9.79	9.85	10.08	10.12	10.08	9.99	10.07	10.00	10.00	10.00	100.00
Deep rotational slides (DRS)											
0–10	**1.26**	0.97	0.90	0.95	1.96	1.63	0.90	0.45	0.45	0.39	9.87
10–20	1.96	**1.32**	1.10	0.93	1.13	1.62	0.96	0.50	0.25	0.19	9.96
20–30	0.98	1.24	**1.55**	1.21	1.08	1.49	1.11	0.81	0.27	0.20	9.94
30–40	1.20	1.30	1.52	**1.39**	1.00	0.91	1.10	0.86	0.42	0.23	9.93
40–50	1.28	1.25	0.93	1.24	**1.46**	0.80	0.89	1.01	0.91	0.29	10.06
50–60	0.54	0.75	1.31	1.32	0.92	**0.85**	1.48	1.21	1.30	0.43	10.11
60–70	0.90	0.50	1.09	1.39	1.54	0.68	**0.90**	1.15	1.30	0.64	10.10
70–80	0.56	1.48	0.62	1.03	0.71	0.56	0.68	**1.27**	1.86	1.24	10.01
80–90	0.79	0.86	0.62	0.63	0.20	0.69	1.14	1.47	**1.75**	1.83	10.00
90–100	0.42	0.23	0.32	0.08	0.06	0.76	0.83	1.29	1.48	**4.56**	10.01
Σ Map 2	9.87	9.90	9.96	10.17	10.07	10.00	10.01	10.02	10.00	10.00	100
Shallow rotational slides (SRS)											
0–10	**1.35**	1.43	1.32	1.34	1.27	1.02	0.76	0.69	0.49	0.15	9.82
10–20	2.01	**1.69**	1.59	0.93	0.84	0.96	0.83	0.56	0.27	0.34	10.03
20–30	1.41	1.78	**1.57**	1.53	0.70	1.04	0.78	0.56	0.34	0.39	10.11
30–40	1.93	1.15	0.89	**1.49**	0.51	1.12	0.78	0.58	0.73	0.83	10.01
40–50	1.08	1.14	1.36	0.95	**0.82**	0.90	1.02	0.96	0.90	0.87	9.99
50–60	0.73	0.85	0.94	1.30	1.19	**0.90**	0.93	1.16	1.02	0.95	9.99
60–70	0.59	0.63	1.00	1.02	1.80	0.95	**1.09**	1.23	0.82	0.89	10.01
70–80	0.35	0.95	0.81	0.84	1.67	1.00	1.15	**1.23**	1.10	0.90	10.01
80–90	0.24	0.23	0.46	0.46	0.97	1.64	1.32	1.38	**1.85**	1.49	10.02
90–100	0.20	0.14	0.05	0.17	0.28	0.48	1.35	1.66	2.49	**3.18**	10.00
Σ Map 2	9.90	10.00	9.98	10.02	10.05	10.02	10.01	10.00	10.01	10.00	100.00
Shallow translational slides (STS)											
0–10	**5.22**	1.29	0.93	0.72	0.49	0.40	0.33	0.38	0.10	0.06	9.92
10–20	2.72	**2.37**	1.43	0.90	0.93	0.59	0.33	0.19	0.31	0.25	10.01
20–30	1.19	2.72	**2.22**	0.91	0.51	0.54	0.73	0.42	0.37	0.38	10.00
30–40	0.51	1.56	1.94	**1.35**	0.70	0.86	0.79	1.16	0.37	0.74	9.98
40–50	0.17	1.18	1.20	1.25	**1.38**	1.25	0.79	1.63	0.71	0.44	10.01

Table 6 (continued)

Map 1 (1983) \ Map 2 (2010)	0–10	10–20	20–30	30–40	40–50	50–60	60–70	70–80	80–90	90–100	Σ Map 1
50–60	0.08	0.45	1.15	1.90	1.63	**0.99**	1.40	0.66	1.15	0.65	10.06
60–70	0.03	0.28	0.67	0.97	2.29	1.18	**1.51**	0.74	1.24	1.09	10.00
70–80	0.01	0.11	0.34	1.16	1.17	1.44	1.67	**1.56**	1.22	1.33	10.00
80–90	0.00	0.01	0.09	0.67	0.60	2.24	1.60	1.47	**1.55**	1.79	10.01
90–100	0.00	0.00	0.01	0.14	0.28	0.53	0.99	1.80	2.97	**3.29**	10.01
Σ Map 2	9.94	9.98	9.97	9.97	9.97	10.01	10.13	10.02	10.00	10.01	100.00

Bold value cells represent the percentage of the study area equally classified in each pair of landslide susceptibility maps

Table 7 Kappa values resulting from comparison of classified landslide susceptibility maps built with 1983 and 2010 event-based landslide inventories

	Ev-B 1983 vs Ev-B 2010	DRS 1983 vs DRS 2010	SRS 1983 vs SRS 2010	STS 1983 vs STS 2010
Kappa index	0.06101	0.07013	0.05748	0.12696
Kappa location	0.06131	0.07035	0.0576	0.12722
Kappa histogram	0.99513	0.99692	0.99797	0.998
Fraction equally classified	0.15	0.16	0.15	0.21

The analysis of the landslide probability-density distribution showed that landslides smaller than 100 m^2 have a slightly higher probability of occurrence when associated to the historical inventory compared to their association with the 1983 and 2010 event-based landslide inventories. This result is unexpected given our prior knowledge that in the north of Lisbon region, small landslides are typically lost soon after their occurrence due to erosion or human intervention, especially in areas dominated by weak rocks or exposed to more intensive agricultural practices (Oliveira et al. 2017). A possible explanation for this result is related to the timing of the detailed geomorphological fieldwork, which is the basis of the historical landslide inventory map for the GPR basin. Landslide mapping started mid-2006 and in this year three new rainfall-triggered landslide events were recorded in the Lisbon region (20 March, 25–27 October, and 28 November): the first two related to critical rainfall sequences of 4–10 days (i.e., short-duration intense rainfall conditions), and the latter to a long-lasting rainfall 40-day period (Zêzere et al. 2008). These events regionally generated a large number of shallow slides that were mapped during the fieldwork and included in the historical landslide inventory map of the study area, thus increasing the number of landslides smaller than 100 m^2. We did not use this information to investigate the short duration events that occurred in the period from March to November 2006 because, at that time, it was not possible to associate all the landslides to a specific rainfall-triggered landslide event.

The landslide probability-density distribution also showed the potential for occurrence of landslide events triggered by rainfall critical conditions more severe than the ones associated to the 1983 and 2010 landslide event at the GPR basin, which is confirmed
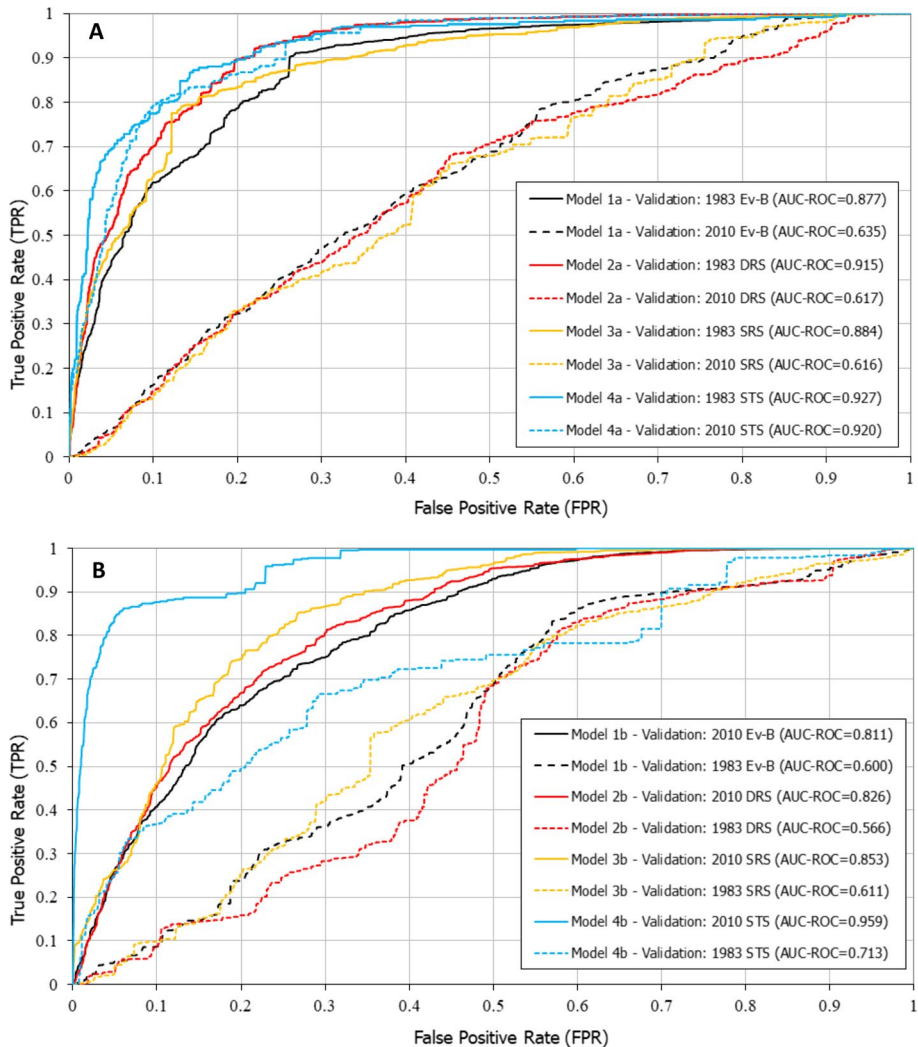
Fig. 8 ROC curves and AUC-ROC values of landslide susceptibility models based on different rainfall event-based landslide inventories: **A** Models built with the 1983 rainfall event-based landslide inventory; **B** Models built with the 2010 rainfall event-based landslide inventory. Filled lines represent the model adjustment and dashed lines the model independent validation. Ev-B, Event-Based; DRS, Deep-seated rotational slides; SRS, Shallow rotational slides; STS, Shallow translational slides

by the progressive detachment to the right side of the historical landslide inventory probability distribution curve in Fig. 6B, namely for landslide magnitudes greater than $L_A > 1000$–2000 m^2. This could be explained if we consider that the geomorphological historical landslide inventories may be the result of the cumulative effects of many landslide events over a period of tens, hundreds, or thousands of years (Guzzetti et al. 2012) and by the above mentioned fact that smaller landslides are typically lost shortly after their occurrence, which could introduce some possible bias related to the weight of the deep-seated landslides in the historical landslide inventory.
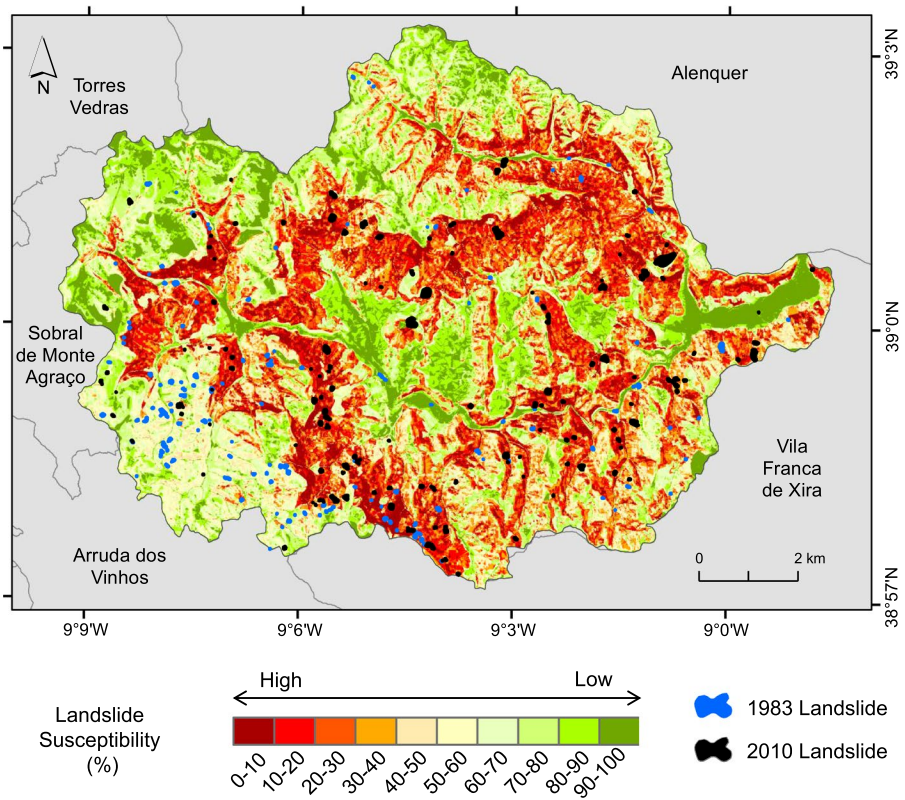
Fig. 9 Landslide susceptibility map based on the historical landslide inventory
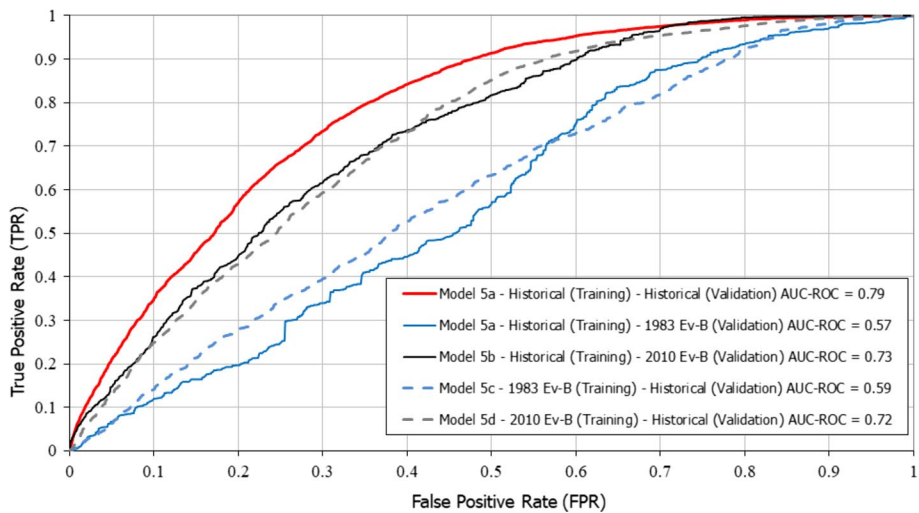
Fig. 10 ROC curves and AUCROC values of landslide susceptibility models based on the historical landslide inventory and rainfall event-based landslide inventories. Filled lines represent the model adjustment and dashed lines the model independent validation. Ev-B = Event-Based
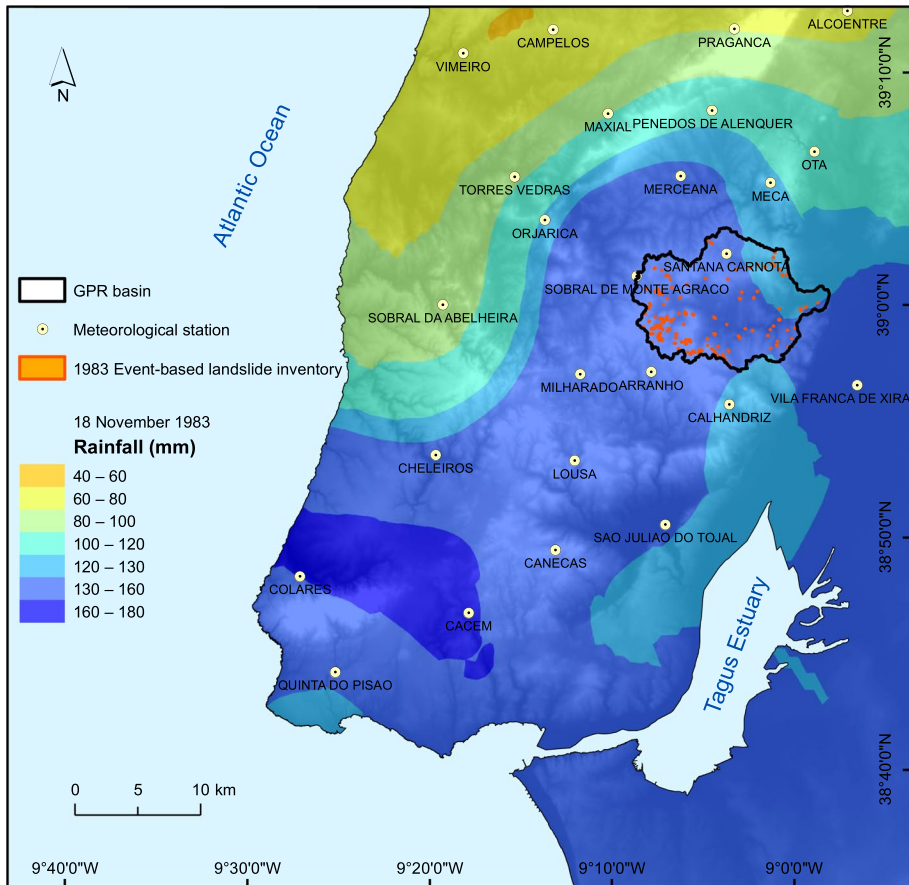
Fig. 11 Spatial interpolation (cokriging) of rainfall records during the 18 November 1983 landslide event in the Lisbon region

The larger landslides included in the historical landslide inventory were identified just below the contact between LU9 (older clay and marl complex gentle slopes) with the upper slope LU7 (compact coralline limestone rock walls). A particular hydrological context favors the development of large landslides in such an upslope position and it may be related to the development of a perched water table in the limestone (UL7) after heavy rainfall over the impermeable clay and marls lithological unit (Coelho 1979). This promotes the retention of water, which is later absorbed by less permeable formations (Ferreira and Zêzere 1997).

Lastly, we cannot neglect the possibility that larger and older landslides than those occurred during the 1983 and 2010 landslide events may have been triggered by earthquakes rather than rainfall. Nevertheless, neither during fieldwork nor in previous works (Vaz and Zêzere 2016) any earthquake-triggered landslide was reported for this study area. In addition, in the north of Lisbon region, the larger complex deep-seated landslide documented as rainfall-triggered (around 180,000 m^2) occurred in 1979 in Calhandriz, near the study area, and in a similar geomorphological context (Ferreira et al. 1987; Zêzere et al. 1999a). The size of this landslide is in line with larger landslides registered in the GPR

basin historical landslide inventory. Only two deep-seated rotational slides mapped in the GPR basin surpass that value, but not exceeding 262,194 m^2 and not corresponding to the unique landslide cases with the main landslide scarp at higher slope positions closer to the top. Therefore, we admit that in GPR basin landslides included in the historical landslide inventory map were triggered by rainfall.

5.2 How reliable can be an event-based landslide susceptibility map?

Independently of the landslide type used for training and validation, the landslide susceptibility models built with the event-based inventories showed to be ineffective in validating other event-based landslide inventories, as well as the historical landslide inventory. This was found to be true for the specific geological/geomorphological context of the GPR basin, where contrasting rainfall critical conditions and hydrological mechanisms can trigger the same type of landslides but varying in size and spatially constrained by different landslide predisposing conditions, particularly lithology and soil type.

Although we did not remove the triggering effect that may control the spatial distribution of landslides, the results for our study area do not support the idea that a common pattern of landslide susceptibility exists for a certain region, regardless of which landslide event is used to build the susceptibility model (Lee and Chung 2017). This is contrary to what is known for other study areas and landslide types (e.g., Lombardo et al. 2018; Knevels et al. 2020). Although we recognize that the spatial distribution of inventoried landslides may be strongly influenced by the spatial distribution of the rainfall event, which is particularly relevant for spatial analyses of event-based inventories, the small size of the study area results in less relevant differences in the spatial patterns of regional rainfall trigger events, particularly those associated with long-lasting rainfall periods. The studied landslide events were triggered by contrasting rainfall critical conditions, which regulate different hydrological mechanisms for landslide initiation and generates distinct associations with landslide predisposing factors. The later was inferred by the contrasting information values of slope and lithological unit for both event-based susceptibility models (Table 3), revealing, as before (e.g., Zêzere et al. 2015), the strong influence of regional geologic and geomorphologic conditions on the slope instability system.

The use of a single event-based landslide inventory to assess landslide susceptibility has been previously recognized as a potential source of bias in landslide susceptibility modeling (Bhandary et al. 2013). This bias may be encompassed by considering a multitemporal approach, which captures more information about the geoenvironmental predisposing conditions that lead to slope instability in a certain study area over time (Bhandary et al. 2013; Mondini and Chang 2014; Persichillo et al. 2017; Reichenbach et al. 2018).

5.3 How appropriate can be an event-based landslide inventory map to independently validate a landslide susceptibility map?

The predictive results of the landslide susceptibility model, based on the historical landslide inventory database (models 5a and 5b) and validated with independent event-based landslide inventories, differs substantially in the study area. The model with the worst prediction is 5a, which was validated with the 1983 event-based inventory. This poor result points out the exceptionality of the spatial distribution of the landslides triggered in 1983, which is not captured by the statistical relationship between the set of landslide predisposing conditions and the landslides historically registered. Furthermore, the results reveal

two complementary sources of uncertainty: the first is related to the use of incomplete historical landslide inventories to assess landslide susceptibility; and the second is associated with the misleading predictive capacity of landslide susceptibility models based on historical landslide inventories when validated with in"dependent" event-based landslide inventory maps (e.g. model 5b validated with the 2010 event-based landslide inventory map). Indeed, the 2010 event-based inventory is relatively similar to the historical inventory, which may generate optimistic results.

Regarding these possible causes of uncertainty, limitations in the landslide inventory have been recognized as a major source of error in landslide susceptibility maps (Fell et al. 2008; Stanley and Kirschbaum 2018; Steger et al. 2017). This is due to the challenge of ensuring the complete identification of historical landslide deposits, especially older ones, which are frequently buried or partially dismantled by subsequent landslide events, partially or totally covered by forest, and partially or totally removed by erosion or human activities such as agriculture and forest practices (Corominas et al. 2014; Guzzetti et al. 2012). This potential source of error is further transferred to data-driven landslide susceptibility predictions, which are completely dependent on the statistical relationships established between the set of geoenvironmental factors assumed as predisposing conditions to slope instability and the available landslide inventory. Although recognized that any event-based landslide inventory map may be suitable to evaluate the predictive capability of landslide susceptibility models, it should be used with caution. The reliability of such evaluations depends on both the pattern, extent and magnitude of the rainfall triggering conditions and the pattern of the geoenvironmental factors that control landslide susceptibility (Reichenbach et al. 2018).

6 Conclusions

In this work, we evaluated and discussed potential sources of uncertainty that may arise from using rainfall-triggered event-based landslide inventories to assess landslide susceptibility in regions where landslides can be triggered by contrasting critical rainfall conditions, including short-duration intense rainfall events or long-lasting rainfall periods. In the study area, the same type of landslides can be triggered by contrasting rainfall critical conditions, but with varying sizes. Landslides increase in size when triggered by long-lasting rainfall critical conditions and are spatially constrained by different landslide predisposing conditions, particularly slope, lithology, and soil type. The study area's event-based landslide susceptibility maps showed that the landslide susceptibility models were not fully validated with the contrasting event-based landslide inventory maps that were not used for training. This suggests that these landslide susceptibility maps may not be entirely reliable. In addition, the results of the landslide susceptibility models based on the historical landslide inventory, which were validated with independent event-based landslide inventory maps, are significantly different and indicate the presence of additional sources of uncertainty. These may arise from the possible incompleteness of the historical landside inventory and an overestimation of the predictive capacity of the landslide susceptibility model due to a validation using a not entirely independent landslide inventory.

In addition to the importance of having a robust historical landslide inventory map, this work aims to contribute to a better knowledge of regional landslide susceptibility patterns based on contrasting rainfall-trigger conditions, providing valuable information to minimize exposure, which is fundamental for risk assessment; to design regional landslide early

warning systems for specific rainfall-triggered landslide events, working as a risk mitigation tool (keeping people away from the dangerous areas in case of expected landslides occurrence); and to improve the response and preparedness of civil protection services/agents (evacuation actions to protect local population and non-stationary assets).

Declarations

References

Alonso EE, Pineda J, Cardoso R (2010) Degradation of marls; two case studies from the Iberian Peninsula. In: Calcaterra D, Parise M (eds) Weathering as a predisposing Factor to Slope Movements, vol 23. The Geological Society of London, pp 47–75

Ardizzone F, Cardinali M, Galli M, Guzzetti F, Reichenbach P (2007) Identification and mapping of recent rainfall-induced landslides using elevation data collected by airborne Lidar. Nat Hazards Earth Syst Sci 7(6):637–650. https://doi.org/10.5194/nhess-7-637-2007

Ardizzone F, Fiorucci F, Santangelo M, Cardinali M, Mondini AC, Rossi M, Reichenbach P, Guzzetti F (2013) Very-high resolution stereoscopic satellite images for landslide mapping. In: Margottini C, Canuti P, Sassa K (eds) Landslide science and practice, vol 1. Springer, Berlin Heidelberg, pp 95–101

Bevacqua E, De Michele C, Manning C, Couasnon A, Ribeiro AFS, Ramos AM, Vignotto E, Bastos A, Blesić S, Durante F, Hillier JK, Oliveira SC, Pinto JG, Ragno E, Rivoire P, Saunders K, van der Wiel K, Wu W, Zhang T, Zscheischler J (2021) Guidelines for studying diverse types of compound weather and climate events. Earth's Fut 9:e2021EF002340. https://doi.org/10.1029/2021EF002340

Bhandary NP, Dahal RK, Timilsina M, Yatabe R (2013) Rainfall event-based landslide susceptibility zonation mapping. Nat Hazards 69(1):365–388

Bornaetxea T, Remondo J, Bonachea J, Valenzuela P (2023) Exploring available landslide inventories for susceptibility analysis in Gipuzkoa province (Spain). Nat Hazards 118:2513–2542. https://doi.org/10.1007/s11069-023-06103-w

Carrara A, Catalano E, Valvo MS, Reali C, Merenda L, Rizzo V (1977) Landslide morphometry and typology in two zones, Calabria, Italy. Bull Int as Eng Geol 16:8–13. https://doi.org/10.1007/BF02591433

Chang K, Chiang S, Chen Y, Mondini AC (2014) Modeling the spatial occurrence of shallow landslides triggered by typhoons. Geomorphology 208:137–148. https://doi.org/10.1016/j.geomorph.2013.11.020

Chen M, Tang C, Xiong J, Shi Q, Li N, Gong LF, Wang XD, Tie Y (2020) The long-term evolution of landslide activity near the epicentral area of the 2008 Wenchuan earthquake in China. Geomorphology 367:107317. https://doi.org/10.1016/j.geomorph.2020.107317

Coelho AG (1979) Engineering geological evaluation of slope stability for urban planning and construction. Bull Int as Eng Geol 19:75–78

Corominas J, Van Westen C, Frattini P, Cascini L, Malet J-P, Fotopoulou S, Catani F, Van Den Eeckhaut M, Mavrouli O, Agliardi F, Pitilakis K, Winter MG, Pastor M, Ferlisi S, Tofani V, Herva J, Smith JT (2014) Recommendations for the quantitative analysis of landslide risk. Bull Eng Geol Environ 73:209–263. https://doi.org/10.1007/s10064-013-0538-8

Cruden D, Varnes D (1996) Landslides types and processes, in landslides investigation and mitigation. In: Turner A, Schuster R (eds) Transportation research board. National Academic Press, Washington DC, pp 36–75

Dai FC, Lee CF (2003) A spatiotemporal probabilistic modeling of storm-induced shallow landsliding using aerial photographs and logistic regression. Earth Surf Process Landforms 28(5):527–545. https://doi.org/10.1002/esp.456

Fell R, Corominas J, Bonnard C, Cascini L, Leroi E, Savage WZ (2008) Guidelines for landslide susceptibility, hazard and risk zoning for land use planning. Eng Geol 102(3–4):85–98. https://doi.org/10.1016/j.enggeo.2008.03.022

Ferreira AB, Zêzere JL (1997) Portugal and the Portuguese Atlantic Islands. In: Embleton C, Embleton-Hamann C (eds) Geomorphological Hazards of Europe, developments in Earth surface processes, vol 5. Elsevier, Amsterdam, pp 391–407

Ferreira A, Zêzere J, Rodrigues M (1987) Instabilite des versants dans la region au nord e Lisbonne. Essai de cartographie geomorphologique. Finisterra XXII 22(44):227–246

Ferreira A (1984) Mouvements de terrain dans la region au nord de Lisbonne. Condition morphostructurales et climatiques. In: Mouvements de terrain, Paris, pp 485–494

Fiorucci F, Cardinali M, Carlà R, Rossi M, Mondini AC, Santurri L, Ardizzone F, Guzzetti F (2011) Seasonal landslide mapping and estimation of landslide mobilization rates using aerial and satellite images. Geomorphology 129(1–2):59–70. https://doi.org/10.1016/j.geomorph.2011.01.013

Galli M, Ardizzone F, Cardinali M, Guzzetti F, Reichenbach P (2008) Comparing landslide inventory maps. Geomorphology 94(3–4):268–289. https://doi.org/10.1016/j.geomorph.2006.09.023

Garcia RAC (2002) Avaliação do risco de movimentos de vertente na depressão da Abadia. Mestrado em Geografia Física e Ambiente, Faculdade de Letras, Departamento de Geografia, Universidade de Lisboa (in Portuguese)

Gariano SL, Verini Supplizi G, Ardizzone F, Salvati P, Bianchi C, Morbidelli R, Saltalippi C (2021) Long-term analysis of rainfall-induced landslides in Umbria, central Italy. Nat Hazards 106:2207–2225. https://doi.org/10.1007/s11069-021-04539-6

Ghosh S, van Westen CJ, Carranza EJM, Jetten VG, Cardinali M, Rossi M, Guzzetti F (2012) Generating event-based landslide maps in a data-scarce Himalayan environment for estimating temporal and magnitude probabilities. Eng Geol 128:49–62

Godinho SF (1984) Aspectos meteorológicos das inundações de Novembro de 1983. INMG, Lisboa (in Portuguese)

Gostelow P (1991) Rainfall and landslides, in Prevention and control of landslide and other mass movements. In: Almeida-Teixiera M, Fantechi R, Oliveira R, Gomes Coelho A (eds) Commis. European Communities, pp 139–161

Guzzetti F, Cardinali M, Reichenbach P, Carrara A (2000) Comparing landslide maps: a case study in the upper Tiber River basin, central Italy. Environ Manag 25(3):247–263. https://doi.org/10.1007/s002679910020

Guzzetti F, Peruccacci S, Rossi M, Stark CP (2007) Rainfall thresholds for the initiation of landslides in central and southern Europe. Meteorol Atmos Phys 98(3–4):239–267. https://doi.org/10.1007/s00703-007-0262-7

Guzzetti F, Mondini AC, Cardinali M, Fiorucci F, Santangelo M, Chang KT (2012) Landslide inventory maps: new tools for an old problem. Earth-Sci Rev 112(1–2):42–66

Harp EL, Keefer DK, Sato HP, Yagi H (2011) Landslide inventories: the essential part of seismic landslide hazard analyses. Eng Geol 122(1–2):9–21. https://doi.org/10.1016/j.enggeo.2010.06.013

Iverson RM (2000) Landslide triggering by rain infiltration. Water Resorces Res 36(7):1897–1910

Jesus CC, Oliveira SC, Sena C, Marques F (2014) Landslides from the Arruda dos Vinhos region in a regional and a local perspective: preliminary results. Comun Geol 101:2014

Jesus CC, Oliveira SC, Sena C, Marques F (2018) Understanding constraints and triggering factors of landslides: regional and local perspectives on a drainage basin. Geosciences. https://doi.org/10.3390/geosciences8010002

Jiménez-Valverde A (2012) Insights into the area under the receiver operating characteristic curve (AUC) as a discrimination measure in species distribution modelling. Glob Ecol Biogeogr. https://doi.org/10.1111/j.1466-8238.2011.00683.x

Knevels R, Petschko H, Proske H, Leopold P, Maraun D, Brenning A (2020) Event-based landslide modeling in the Styrian Basin, Austria: accounting for time-varying rainfall and land cover. Geosciences 10:217. https://doi.org/10.3390/geosciences10060217

Kullberg J, Rocha R, Soares A, Rey J, Terrinha P, Callapez P, Martins L (2006) A Bacia Lusitaniana: Estratigrafia, paleogeografia e tectónica. In: Dias R, Araújo A, Terrinha P, Kullberg J (eds) Geologia de Portugal no contexto da Ibéria, Universidade de Évora, pp 317–368

Lee C-T, Chung C-C (2017) Common patterns among different landslide susceptibility models of the same region. In: Mikoš M, Tiwari B, Yin Y, Sassa K (eds) Advancing culture of living with landslides, Vol. 2 Advances in Landslide Science, WLF 2017, Cham, pp 937–942. https://doi.org/10.1007/978-3-319-53498-5_106

Lee C-T, Huang C-C, Lee J-F, Pan K-L, Lin M-L, Dong J-J (2008) Statistical approach to storm event-induced landslides susceptibility. Nat Hazards Earth Syst Sci 8(4):941–960

Lombardo L, Opitz T, Huser R (2018) Point process-based modeling of multiple debris flow landslides using INLA: an application to the 2009 Messina disaster. Stoch Environ Res Risk Assess 32:2179–2198. https://doi.org/10.1007/s00477-018-1518-0

Malamud BD, Turcotte DL, Guzzetti F, Reichenbach P (2004) Landslide inventories and their statistical properties. Earth Surf Process Landforms 29(6):687–711. https://doi.org/10.1002/esp.1064

Martelloni G, Segoni S, Fanti R, Catani F (2012) Rainfall thresholds for the forecasting of landslide occurrence at regional scale. Landslides 9:485–495. https://doi.org/10.1007/s10346-011-0308-2

Mondini AC, Chang K-T (2014) Combining spectral and geoenvironmental information for probabilistic event landslide mapping. Geomorphology 213:183–189

Mondini AC, Guzzetti F, Reichenbach P, Rossi M, Cardinali M, Ardizzone F (2011) Semi-automatic recognition and mapping of rainfall induced shallow landslides using optical satellite images. Remote Sens Environ 115(7):1743–1757. https://doi.org/10.1016/j.rse.2011.03.006

Mondini AC, Viero A, Cavalli M, Marchi L, Herrera G, Guzzetti F (2014) Comparison of event landslide inventories: the Pogliaschina catchment test case, Italy. Nat Hazards Earth Syst Sci 14(7):1749–1759

Murillo-García FG, Alcántara-Ayala I, Ardizzone F, Cardinali M, Fiorucci F, Guzzetti F (2015) Satellite stereoscopic pair images of very high resolution: a step forward for the development of landslide inventories. Landslides 12(2):277–291. https://doi.org/10.1007/s10346-014-0473-1

Oliveira SC, Zêzere JL, Garcia RA (2015a) Structure and characteristics of landslide input data and consequences on landslide susceptibility assessment and prediction capability. In: Landslide Processes, Engineering Geology for Society and Territory, Vol. 2, Springer, Cham, pp 189–192, https://doi.org/10.1007/978-3-319-09057-3_24

Oliveira SC, Zêzere JL, Catalão J, Nico G (2015b) The contribution of PSInSAR interferometry to landslide hazard in weak rock-dominated areas. Landslides 12(4):703–719. https://doi.org/10.1007/s10346-014-0522-9

Oliveira SC, Zêzere JL, Lajas S, Melo R (2017) Combination of statistical and physically based methods to assess shallow slide susceptibility at the basin scale. Nat Hazards Earth Syst Sci 17(7):1091–1109. https://doi.org/10.5194/nhess-17-1091-2017

Oliveira SC, Zêzere JL, Garcia RAC (2014) Assessment of rainfall thresholds for landslide triggering in the Rio Grande da Pipa basin, Arruda dos Vinhos. Comun Geol 101

Oliveira SC (2012) Incidência espacial e temporal da instabildiade gemorfológica na bacia do rio Grande da Pipa (Arruda dos Vinhos). Instituto de Geografia e Ordenamento do Território, Universidade de Lisboa (in portuguese)

Palmer AC, Rice JR (1973) The growth of slip surfaces in the progressive failure of over-consolidated clay. Proc Roy Soc Lond A 332:527–548

Pašek J (1975) Landslides inventory. Bull Int as Eng Geol 12:73–74. https://doi.org/10.1007/BF02635432

Pereira S, Garcia RAC, Zêzere JL, Oliveira SC, Silva M (2017) Landslide quantitative risk analysis of buildings at the municipal scale based on a rainfall triggering scenario. Geomat Nat Hazards Risk 8(2):624–648. https://doi.org/10.1080/19475705.2016.1250116

Persichillo MG, Bordoni M, Meisina C, Bartelletti C, Giannecchini R, Avanzi GD, Galanti Y, Barsanti M, Cevasco A, Brandolini P, Galve JP (2017) Remarks on the role of landslide inventories in the statistical methods used for the landslide susceptibility assessment. In: Mikoš M, Tiwari B, Yin Y, Sassa K

(eds) Advancing culture of living with landslides, Vol. 2 Advances in Landslide Science, WLF 2017. Springer, Cham, pp 759–766. https://doi.org/10.1007/978-3-319-53498-5_87

Ramos AM, Trigo RM, Liberato MLR (2014) A ranking of high-resolution daily precipitation extreme events for the Iberian Peninsula. Atmos Sci Lett 15(4):328–334. https://doi.org/10.1002/asl2.507

Reichenbach P, Rossi M, Malamud BD, Mihir M, Guzzetti F (2018) A review of statistically-based landslide susceptibility models. Earth-Sci Rev 180(March):60–91. https://doi.org/10.1016/j.earscirev.2018.03.001

Ribeiro A, Antunes MT, Ferreira MP, Rocha RB, Soares AF, Zbyszewski G, Moitinho De Almeida F, Carvalho D, Monteiro JH (1979) Introduction à la géologie Générale du Portugal, Serviços Geológicos de Portugal, Lisboa

Santangelo M, Marchesini I, Bucci F, Cardinali M, Fiorucci F, Guzzetti F (2015) An approach to reduce mapping errors in the production of landslide inventory maps. Nat Hazards Earth Syst Sci 15(9):2111–2126. https://doi.org/10.5194/nhess-15-2111-2015

Sidle RC, Bogaard TA (2016) Dynamic earth system and ecological controls of rainfall-initiated landslides. Earth-Sci Rev 159:275–291. https://doi.org/10.1016/j.earscirev.2016.05.013

Stanley TA, Kirschbaum DB (2018) Effects of Inventory Bias on Landslide Susceptibility Calculations. In: Proceedings of the 3rd North American symposium on landslides. AEG Publishing, Roanoke, VA, United States, pp 794–806

Steger S, Brenning A, Bell R, Glade T (2017) The influence of systematically incomplete shallow landslide inventories on statistical susceptibility models and suggestions for improvements. Landslides 14:1767–1781. https://doi.org/10.1007/s10346-017-0820-0

Sterlacchini S, Ballabio C, Blahut J, Masetti M, Sorichetta A (2011) Spatial agreement of predicted patterns in landslide susceptibility maps. Geomorphology 125(1):51–61. https://doi.org/10.1016/j.geomorph.2010.09.004

Stumpf A, Malet JP, Delacourt C (2017) Correlation of satellite image time-series for the detection and monitoring of slow-moving landslides. Remote Sens Environ 189:40–55. https://doi.org/10.1016/j.rse.2016.11.007

Su C, Wang L, Wang X, Huang Z, Zhang X (2015) Mapping of rainfall-induced landslide susceptibility in Wencheng, China, using support vector machine. Nat Hazards 76:1759–1779. https://doi.org/10.1007/s11069-014-1562-0

Van Asch TWJ, Buma J, Van Beek LPH (1999) A view on some hydrological triggering systems in landslides. Geomorphology 30:25–32

Van Den Eeckhaut M, Poesen J, Govers G, Verstraeten G, Demoulin A (2007) Characteristics of the size distribution of recent and historical landslides in a populated hilly region. Earth Planet Sci Lett 256(3–4):588–603. https://doi.org/10.1016/j.epsl.2007.01.040

Van Den Eeckhaut M, Kerle N, Hervás J, Supper R (2013) Mapping of landslides under dense vegetation cover using object-oriented analysis and LiDAR derivatives. In: Margottini C, Canuti P, Sassa K (eds) Landslide science and practice, vol 1. Springer, Berlin Heidelberg, pp 103–109

Vaz T, Zêzere JL (2016) Landslides and other geomorphologic and hydrologic effects induced by earthquakes in Portugal. Nat Hazards 81(1):71–98. https://doi.org/10.1007/s11069-015-2071-5

Vaz T, Zêzere JL, Pereira S, Oliveira SC, Garcia RAC, Quaresma I (2018) Regional rainfall thresholds for landslide occurrence using a centenary database. Nat Hazards Earth Syst Sci 18:1037–1054. https://doi.org/10.5194/nhess-18-1037-2018

Vicente-Serrano SM, Trigo RM, López-Moreno JI, Liberato MLR, Lorenzo-Lacruz J, Beguería S, Morán-Tejeda E, El Kenawy A (2011) Extreme winter precipitation in the Iberian Peninsula in 2010: anomalies, driving mechanisms and future projections. Clim Res 46(1):51–65. https://doi.org/10.3354/cr00977

Visser H, Nijs T (2006) The map comparison kit. Environ Model Softw 21:346–358

Yin KL, Yan TZ (1988) Statistical prediction models for slope instability of metamorphic rocks. In: Bonnard C (ed) Landslides. Balkema, Rotterdam, pp 1269–1272

Zbyszewski G, Assunção CT (1965) Notícia explicativa da folha 30-D (Alenquer). Carta Geológica de Portugal, Serviços Geológicos de Portugal, Lisboa (in portuguese)

Zêzere JL, Trigo RM (2011) Impacts of the North Atlantic Oscillation on landslides. In: Vicente-Serrano S, Trigo R (eds) Hydrologicall, Socioeconomic and ecological impacts of the North Atlantic Oscillation in the Mediterranean Region. Springer, Advances in Global Change Research, vol 46. Springer, Dordrecht, pp 199–212. https://doi.org/10.1007/978-94-007-1372-7_14

Zêzere JL, Ferreira AB, Rodrigues ML (1999a) The role of conditioning and triggering factors in the occurrence of landslides: a case study in the area north of Lisbon (Portugal). Geomorphology 30(1–2):133–146. https://doi.org/10.1016/S0169-555X(99)00050-1

Zêzere JL, Ferreira AB, Rodrigues ML (1999b) Landslides in the north of Lisbon Region (Portugal): conditioning and triggering factors. Phys Chem Earth 24(10):925–934

Zêzere JL, Trigo RM, Trigo IF (2005) Shallow and deep landslides induced by rainfall in the Lisbon region (Portugal): assessment of relationships with the North Atlantic Oscillation. Nat Hazards Earth Syst Sci 5:331–344

Zêzere JL, Trigo RM, Fragoso M, Oliveira SC, Garcia RAC (2008) Rainfall-triggered landslides in the Lisbon region over 2006 and relationships with the North Atlantic Oscillation. Nat Hazards Earth Syst Sci 8(3):483–499. https://doi.org/10.5194/nhess-8-483-2008

Zêzere JL, Vaz T, Pereira S, Oliveira SC, Marques R, Garcia RAC (2015) Rainfall thresholds for landslide activity in Portugal: a state of the art. Environ Earth Sci 73(6):2917–2936. https://doi.org/10.1007/s12665-014-3672-0

Zêzere JL, Pereira S, Melo R, Oliveira SC, Garcia RAC (2017) Mapping landslide susceptibility using data-driven methods. Sci Total Environ 589:250–267. https://doi.org/10.1016/j.scitotenv.2017.02.188

Zêzere JL (1997) Movimentos de vertente e perigosidade geomorfológica na Região a Norte de Lisboa, Doutoramento em Geografia Física. Universidade de Lisboa (in Portuguese)

Zieher T, Perzl F, Rössel M, Rutzinger M, Meißl G, Markart G, Geitner C (2016) A multi-annual landslide inventory for the assessment of shallow landslide susceptibility—two test cases in Vorarlberg, Austria. Geomorphology 259:40–54

Authors and Affiliations

Sérgio C. Oliveira[1,2] (ID) **· José L. Zêzere[1,2] · Ricardo A. C. Garcia[1,2] · Susana Pereira[1,2,3] · Teresa Vaz[1] · Raquel Melo[1,2]**

✉ Sérgio C. Oliveira
cruzdeoliveira@edu.ulisboa.pt

José L. Zêzere
zezere@edu.ulisboa.pt

Ricardo A. C. Garcia
rgarcia@edu.ulisboa.pt

Susana Pereira
sspereira@letras.up.pt

Teresa Vaz
tvaz@campus.ul.pt

Raquel Melo
raquel.melo@edu.ulisboa.pt

[1] Centre of Geographical Studies, Institute of Geography and Spatial Planning, Universidade de Lisboa, Edifício IGOT, Rua Branca Edmée Marques, 1600-276 Lisboa, Portugal

[2] Associate Laboratory TERRA, Lisboa, Portugal

[3] Centre of Studies in Geography and Spatial Planning, Geography Department, Faculty of Arts and Humanities, University of Porto, Via Panorâmica s/n, 4150-564 Porto, Portugal